Cell

Arabidopsis uses distinct coumarins and bacterial pathways for pH-adaptive iron acquisition

Graphical abstract

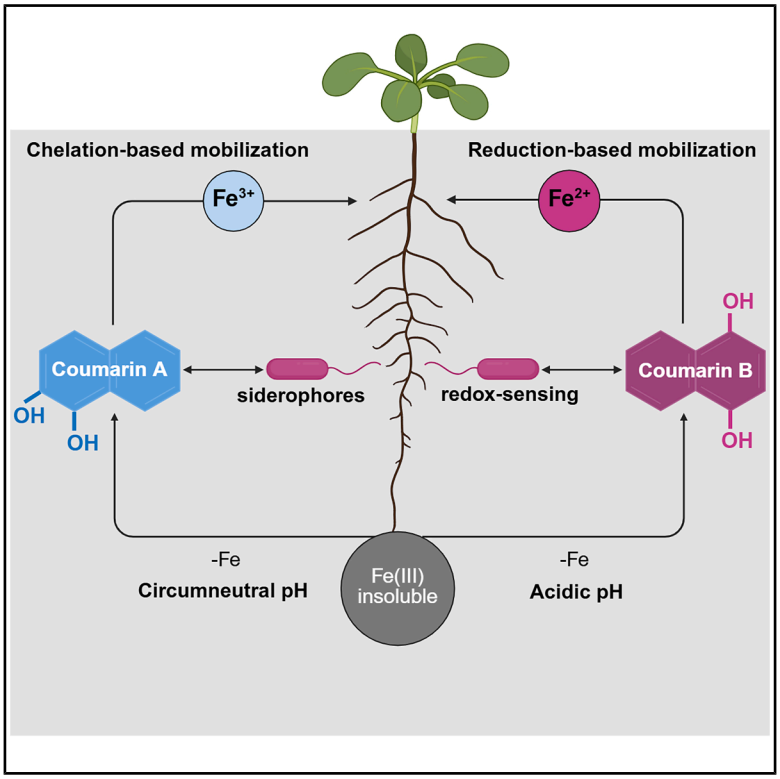

Highlights

- Bacteria rescue *Arabidopsis* Fe deficiency independent of parent soil edaphic factors
- Roots adapt coumarin exudation to determine pH-specific bacterial Fe mobilization
- Coumarins engage conserved bacterial redox or chelation pathways for Fe acquisition
- Plants may co-opt ancient microbial processes to overcome Fe limitation

Authors

Milena Malisic, Charles Copeland, Anton Amrhein, ..., Ruben Garrido-Oter, Ricardo F.H. Giehl, Paul Schulze-Lefert

Correspondence

schlef@mpipz.mpg.de

In brief

Arabidopsis coordinates Fe acquisition with its root microbiota by releasing distinct coumarin chemotypes in response to environmental pH. These root-exuded specialized metabolites interact with root-associated bacteria to mobilize Fe either through bacterial siderophore-dependent chelation at circumneutral pH or through bacterial redox-sensing-controlled reduction at acidic pH.

Malisic et al., 2026, Cell *189*, 1–18
October 15, 2026 © 2026 The Author(s). Published by Elsevier Inc.
https://doi.org/10.1016/j.cell.2026.09.030

CellPress

Please cite this article in press as: Malisic et al., *Arabidopsis* uses distinct coumarins and bacterial pathways for pH-adaptive iron acquisition, Cell (2026), https://doi.org/10.1016/j.cell.2026.09.030

Cell

CellPress
OPEN ACCESS

Article

Arabidopsis uses distinct coumarins and bacterial pathways for pH-adaptive iron acquisition

Milena Malisic,[1,2,8] Charles Copeland,[1,8] Anton Amrhein,[1] Pengfan Zhang,[1,9] Masayoshi Hashimoto,[1,3] Christopher J. Harbort,[1,10] Tak Lee,[1] Yudelsy A. Tandron Moya,[4] Lara Van Dijck,[1,11,12] Niklas Kiel,[1,2] Stanislav Kopriva,[2,6] Sabine Metzger,[2,6] Ruben Garrido-Oter,[1,2,7] Ricardo F.H. Giehl,[4,5] and Paul Schulze-Lefert[1,2,8,13,*]

[1]Department of Plant Microbe Interactions, Max Planck Institute for Plant Breeding Research, 50829 Cologne, Germany
[2]Cluster of Excellence on Plant Sciences (CEPLAS), 50829 Cologne, Germany
[3]Faculty of Agriculture, Shizuoka University, Shizuoka 422-8529, Japan
[4]Molecular plant nutrition, Department of Physiology & Cell Biology, Leibniz Institute of Plant Genetics and Crop Plant Research (IPK), 06466 Gatersleben, Germany
[5]Cluster of excellence on plant sciences (CEPLAS), 06466 Gatersleben, Germany
[6]Institute for Plant Sciences, University of Cologne, 50674 Cologne, Germany
[7]Earlham Institute, Norwich Research Park, Norwich NR4 7UZ, UK
[8]These authors contributed equally
[9]Present address: Innovative Genomics Institute, University of California, Berkeley, Berkeley, CA, USA
[10]Present address: Department of Cellular Microbiology, Max Planck Institute for Infection Biology, Charitéplatz 1, 10117, Berlin, Germany
[11]Present address: Department of Plant Biotechnology and Bioinformatics, Ghent University, 9052 Ghent, Belgium
[12]Present address: VIB Center for Plant Systems Biology, 9052 Ghent, Belgium
[13]Lead contact
*Correspondence: schlef@mpipz.mpg.de
https://doi.org/10.1016/j.cell.2026.09.030

SUMMARY

Iron (Fe) limitation restricts plant growth in diverse soils, and root-associated microbes can alleviate plant Fe starvation. Whether plants integrate the edaphic environment and microbial activities into their Fe uptake strategies remains unclear. We show that bacterium-mediated alleviation of Fe deficiency in *Arabidopsis* functions at varying environmental pH and is taxonomically widespread among root microbiota isolates from soils with different edaphic profiles. This process is regulated by host-controlled and pH-adapted root exudation of different coumarin chemotypes. These exometabolites interact with root-associated bacteria to mobilize Fe either via bacterial siderophore-mediated chelation at circumneutral pH or redox-sensing-controlled, reduction-based pathways at acidic pH. The corresponding bacterial genes are prevalent in the root microbiota, and they likely evolved before the emergence of land plants. Our findings suggest that Fe malnutrition-induced exudation of redox-active metabolites by non-graminaceous plant species is a widespread adaptation for Fe mobilization from soil, mediated by the co-option of ancient microbial processes.

INTRODUCTION

Healthy plants live in close association with diverse root-associated microbial communities, collectively termed the root microbiota.[1–3] These communities are shaped by both the surrounding soil biome and host-derived metabolites, and a small number of bacterial phyla—including *Actinomycetota*, *Bacteroidota*, and *Pseudomonadota*—form a conserved core across plant species and environments.[1,4–6] Core microbiota members contribute to host fitness by promoting pathogen resistance, abiotic stress tolerance, and nutrient acquisition.[7–18] Root-exuded metabolites play central roles in establishing beneficial associations with soil-borne microbes.[9,12,14,15,19–21] In symbiotic relationships, (iso)flavonoids recruit dinitrogen-fixing rhizobia under nitrogen limitation in legumes, while strigolactones mediate arbuscular mycorrhizal interactions under phosphorus limitation in the majority of terrestrial plant species.[13]

Iron (Fe) is an essential micronutrient for plant growth and development, yet its bioavailability is severely constrained in many natural soils.[22,23] In well-aerated soils, and increasingly so with rising soil pH, Fe predominantly occurs as Fe(III) complexed in insoluble ferric (hydr)oxides, rendering it largely inaccessible to plants.[23,24] Plants have evolved two principle strategies, strategy I and strategy II, to acquire this essential nutrient. A

This is an open access article under the CC BY license (http://creativecommons.org/licenses/by/4.0/).
Open access funding enabled and organized by Projekt DEAL.

Please cite this article in press as: Malisic et al., *Arabidopsis* uses distinct coumarins and bacterial pathways for pH-adaptive iron acquisition, Cell (2026), https://doi.org/10.1016/j.cell.2026.09.030

key distinction is that strategy I species (dicotyledons and non-graminaceous monocotyledons) reduce Fe(III) to Fe(II) at the root surface before cellular uptake, whereas strategy II species (graminaceous monocotyledons) acquire Fe(III) directly through specialized chelation mechanisms.[25–27] In the strategy I plant *Arabidopsis thaliana*, reductive import of Fe under bioavailable Fe (avFe) conditions mainly relies on Fe(III) reduction by the ferric-chelate reductase FRO2[28] and subsequent import of Fe(II) via the high-affinity Fe transporter IRON-REGULATED TRANSPORTER 1 (IRT1).[29–32]

In conditions of low Fe bioavailability, Fe uptake in strategy I is supported by Fe deficiency-induced secretion of redox-active specialized metabolites such as coumarins, which mobilize Fe in the rhizosphere.[25,26,30,33–41] In *A. thaliana*, the major Fe-mobilizing coumarins are produced via a linear biosynthesis pathway consisting of four enzymatic steps: first, FERULOYL-CoA 6′-HYDROXYLASE 1 (F6'H1) and coumarin synthase (COSY) produce scopoletin from feruloyl-coenzyme A (CoA)[42,43]; subsequently, the SCOPOLETIN 8-HYDROXYLASE (S8H) hydroxylates scopoletin to yield fraxetin[34,37,41]; and finally, the cytochrome P450 enzyme CYP82C4 hydroxylates fraxetin to yield sideretin.[34] A further coumarin, esculetin, is found in root exudates under Fe limitation, but the biosynthetic steps are still unknown.[30] It is thought that pH-dependent alteration of coumarin profiles exuded into the rhizosphere constitutes an adaptive component of strategy I Fe acquisition.[26,30,44,45] Although coumarin chemotypes, enriched in root exudates under specific pH conditions, contribute to plant Fe nutrition from immobile Fe sources, paradoxically, germ-free plants still exhibit pronounced Fe deficiency.[9,12,30] We have previously shown that this Fe deficiency is rescued by a synthetic community (SynCom) of bacterial root microbiota through interaction with root-secreted fraxetin at circumneutral pH.[9] However, it remains unclear whether and how plants integrate the edaphic environment and root microbiota functions for adaptive Fe acquisition from soils with different pH.

Here, using gnotobiotic systems with the strategy I plant *A. thaliana* and the root commensal *Aquipseudomonas proteolytica* IT466 (Basonym *Pseudomonas proteolytica*, hereafter IT466) as a model system, complemented by synthetic community reconstitution and natural soil experiments, we show that plants integrate environmental pH to tune coumarin exudation enabling flexible recruitment of pH-specific microbiota functions for rhizosphere Fe mobilization under Fe limitation. By combining host genetics, bacterial forward genetics, and targeted gene inactivation with *ex planta* Fe mobilization assays, we identified two distinct mechanisms of Fe mobilization operating at different environmental pH. At circumneutral pH, fraxetin-commensal interactions promote Fe(III) mobilization via a chelation-based mechanism involving the bacterial siderophore pyoverdine (PVD), whereas at acidic pH, sideretin engages bacterial redox-sensing pathways (RoxSR and Anr) for Fe(III) reduction. Using synthetic quinones, we define the *p*-quinone moiety in sideretin as a structural determinant for the latter activity. Transcriptomic profiles of IT466 revealed RoxR-dependent candidate genes implicated in a sideretin redox shuttle for sustained extracellular Fe reduction in acidic conditions. Siderophore production and redox sensing are widespread microbial traits, and we show that Fe deficiency rescue is prevalent among diverse root commensals, irrespective of their edaphic origin.[46–49] Thus, our findings indicate that pH-specific coumarin exometabolites co-opt conserved bacterial functions for pH-adaptive Fe acquisition from soil.

RESULTS

Widespread relief of *A. thaliana* Fe starvation symptoms by root microbiota members at varying pH is largely independent of parent soil Fe bioavailability

To examine whether the root microbiota of *A. thaliana* plants grown in natural soils with different pH and bioavailable Fe differs in the proportion of members capable of rescuing plant Fe deficiency, we tested taxonomically representative bacterial isolates from two root microbiota culture collections: At_{CAS}-RSPHERE[50] from Cologne Agricultural Soil (CAS) and At_{IS}-RSPHERE (this study) from Italian Soil (IS). Compared with IS, CAS has a lower pH and contains more bioavailable Fe.[9]

Isolates were screened in mono-association for their ability to rescue Fe deficiency symptoms of wild-type (WT) Col-0 plants, using a gnotobiotic agar matrix-based growth system[51] with bio-unavailable Fe conditions (unavFe, Fe(III) supplied as $FeCl_3$) under acidic and circumneutral pH (pH 5.7 and pH 7.4; Table S1). After 3 weeks of co-cultivation, Fe deficiency symptoms were assessed by measuring the maximum quantum yield of photosystem II in shoots (F_v/F_m).[52–54] Because germ-free *A. thaliana* plants acquire Fe more efficiently at acidic pH than at circumneutral pH,[30] 50 μM $FeCl_3$ was used to induce Fe deficiency symptoms at acidic pH, compared with 100 μM at circumneutral pH (Figure S1A). Rescuing strains were defined as those that increased plant F_v/F_m under unavFe conditions to ≥50% of the range between the axenic unavFe control (0% rescue) and the axenic avFe control (100% rescue).

Of a total of 133 strains from At_{CAS}-RSPHERE and 113 strains from At_{IS}-RSPHERE, more than 74% of all root-derived bacteria relieved Fe deficiency of the host at a pH of 7.4 (Figures 1A and S1B). Similarly, more than 65% of all root-derived bacteria relieved host Fe deficiency at a pH of 5.7 (Figures 1A and S1C). Rescue activity was observed across all core taxonomic lineages of the root microbiota, including the classes *Actinomycetes*, *Alphaproteobacteria*, *Gammaproteobacteria*, *Bacteroidia*, and *Bacilli* (Figures 1A, 1B, S1B, and S1C). Each of the five bacterial classes with more than one member contained ≥50% rescuing commensals (Figure 1A), with strain-specific rescue activities observed within taxonomic lineages (Figure 1B).

We then selected representative At_{CAS}- and At_{IS}-derived commensals that rescued Fe deficiency under unavFe conditions and tested them under avFe at both pH conditions (Figure 1B; Table S1). None affected the F_v/F_m parameter when Fe was readily available, indicating that the enhanced photosynthetic performance under unavFe reflects improved Fe acquisition rather than general effects on plant physiology (Figure S1D).

Together, these results suggest that the rescue of *A. thaliana* Fe deficiency is a widespread, functionally redundant trait among root commensals that is largely independent of parent soil edaphic factors.

Please cite this article in press as: Malisic et al., *Arabidopsis* uses distinct coumarins and bacterial pathways for pH-adaptive iron acquisition, Cell (2026), https://doi.org/10.1016/j.cell.2026.09.030

CellPress
OPEN ACCESS

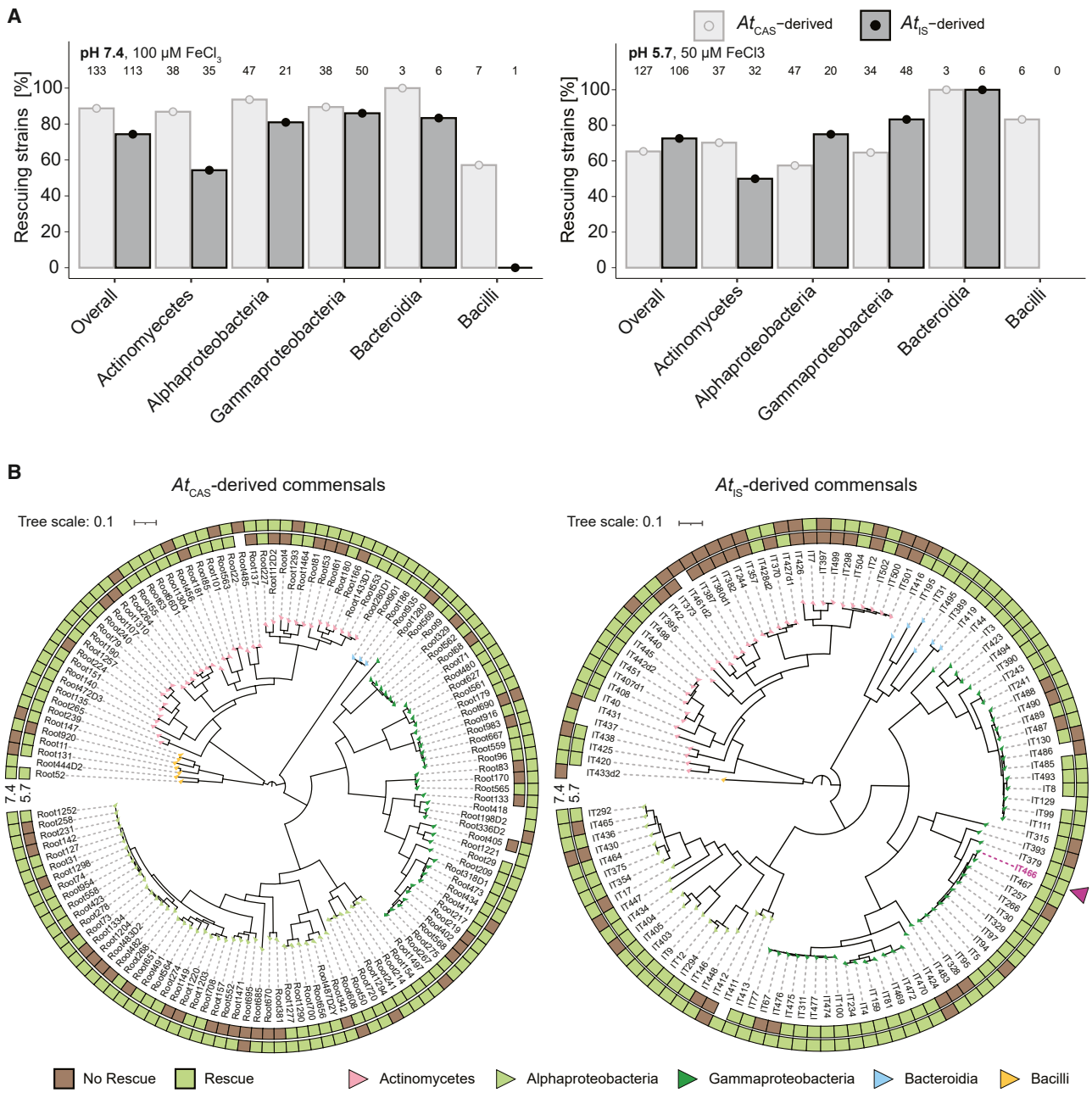

Figure 1. Widespread relief of *A. thaliana* Fe starvation symptoms by root microbiota members at varying pH conditions is largely independent of parent soil Fe bioavailability

(A) Proportion of At_{CAS}- and At_{IS}-derived commensals that rescue host Fe deficiency symptoms across the entire screening set (overall) or per bacterial class (%). Numbers above bars indicate the total count of commensals tested. Screening was performed with 100 µM $FeCl_3$ at pH 7.4 (left panel) or 50 µM $FeCl_3$ at pH 5.7 (right panel) and Fe-deficiency phenotypes assessed based on the maximum quantum efficiency of photosystem II (F_v/F_m). $n = 4$.

(B) Phylogenetic tree of root-associated bacteria from At_{CAS} (left) and At_{IS} (right) culture collections tested at pH 7.4 (outer ring) or pH 5.7 (inner ring). Ring colors indicate Fe deficiency rescue (green) or no rescue (brown); untested strains are uncolored. Branch colors indicate bacterial class. *Pseudomonas proteolytica* IT466 is marked by a purple arrowhead.

FRO2 is dispensable for Fe deficiency rescue of *A. thaliana* by most microbiota members under acidic pH

To dissect the mechanisms underlying commensal-mediated Fe acquisition in *A. thaliana* operating under different environmental pH, we focused on IT466, a *Pseudomonas proteolytica* isolate from the At_{IS}-RSPHERE collection. IT466 was selected for its robust rescue of *A. thaliana* Fe deficiency symptoms at both pH conditions (Figure 1B). The *Pseudomonas* genus is also

Please cite this article in press as: Malisic et al., *Arabidopsis* uses distinct coumarins and bacterial pathways for pH-adaptive iron acquisition, Cell (2026), https://doi.org/10.1016/j.cell.2026.09.030

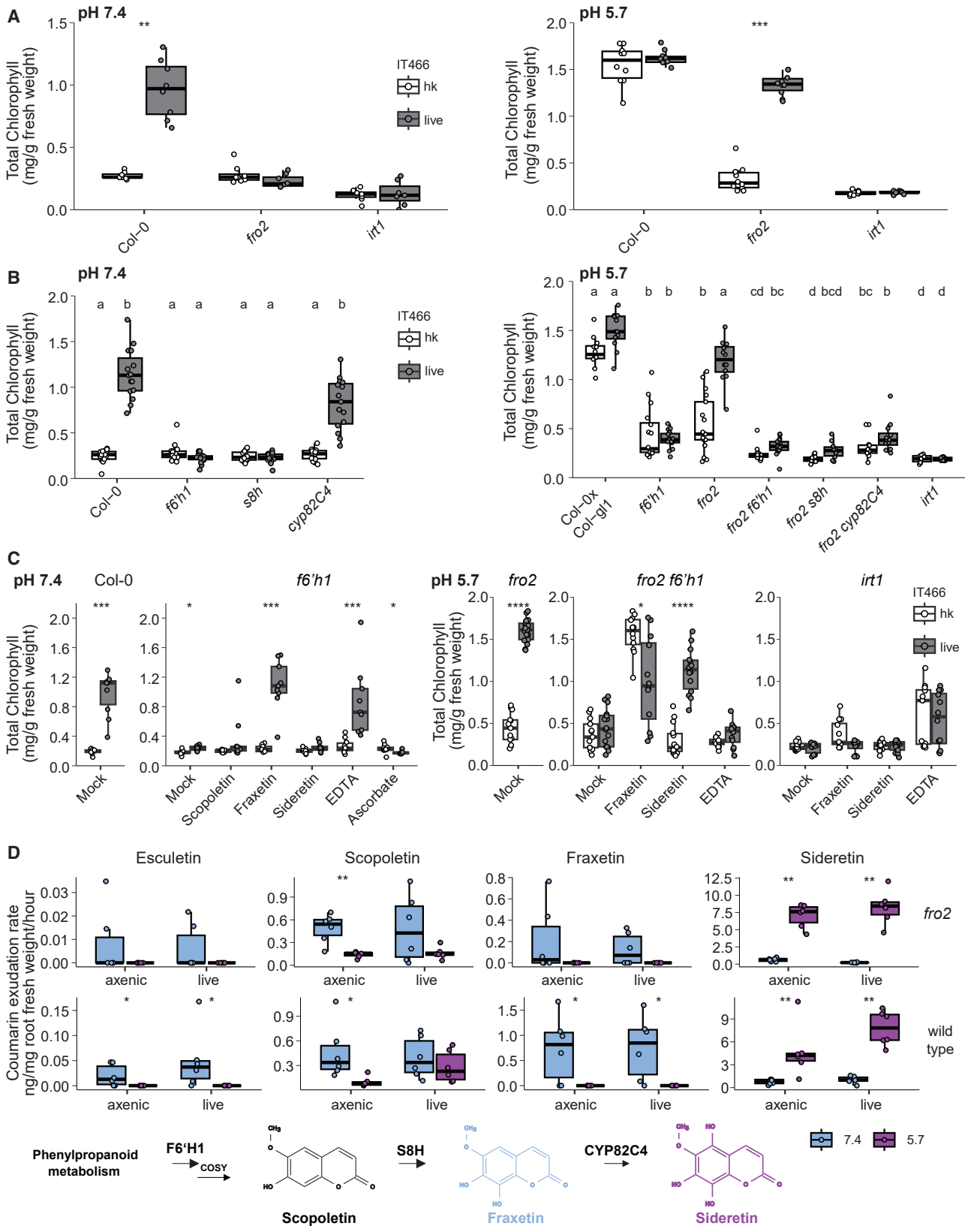

(legend on next page)

Please cite this article in press as: Malisic et al., *Arabidopsis* uses distinct coumarins and bacterial pathways for pH-adaptive iron acquisition, Cell (2026), https://doi.org/10.1016/j.cell.2026.09.030

prevalent in the *A. thaliana* root microbiota and genetically tractable.[5,6]

We validated the screening results (Figures 1B and S1D) by assessing plant performance and shoot Fe status across Fe bioavailabilities. Plants co-cultured with heat-killed IT466 showed severe Fe deficiency under limited unavFe or insufficient Fe, with reduced growth, shoot chlorophyll, and Fe concentrations, compared with avFe (Figures S2A–2D). Deficiency at acidic pH required 50 μM unavFe versus 100 μM at circumneutral pH, confirming greater Fe accessibility to the plant at pH 5.7 than pH 7.4.[30] Consistent with the F_v/F_m parameter, IT466 improved all plant performance parameters at the respective limiting unavFe levels at both pH but not under avFe or insufficient Fe (Figures S2A–2D). At pH 5.7 and 100 μM $FeCl_3$, IT466 slightly increased shoot fresh weight. However, chlorophyll levels did not significantly increase, possibly due to a dilution effect of plant growth[55] (Figures S2B and S2C).

These results indicate that the improved plant performance under unavFe reflects enhanced Fe availability at the roots and allocation to shoots rather than general growth promotion by IT466 (Figures S2A–S2D). At both pH conditions, axenic and heat-killed IT466 treatments showed similar shoot chlorophyll concentrations, indicating that live bacterial activity is required to rescue Fe deficiency (Figure S2E).

To determine how IT466 affects Fe acquisition in *A. thaliana*, we examined whether key Fe-mobilization and uptake genes are required for IT466-mediated rescue of Fe deficiency at acidic and circumneutral pH. We tested mutants defective in Fe(III) reduction (*fro2*), Fe(II) import (*irt1*), and coumarin biosynthesis (*f6'h1*). These experiments used 100 μM $FeCl_3$ to maintain a constant Fe concentration while assessing pH-dependent effects on microbiota-mediated plant Fe acquisition mechanisms.

At circumneutral pH, IT466 failed to rescue *fro2*, *irt1*, and *f6'h1* mutants, indicating that Fe deficiency rescue in WT plants requires FRO2/IRT1-dependent Fe reduction and import as well as coumarin biosynthesis (Figures 2A, 2B, S3A, and S3B). Under acidic pH, however, IT466 rescued *fro2* but not *irt1* or *f6'h1* Fe deficiency (Figures 2A, 2B, S3A, and S3B). Since Fe(III) was the sole Fe source provided in the plant growth medium, these results suggest that at acidic pH, IT466 facilitates reductive import of Fe independently of FRO2 (Figures 2A and S3A).

Consistent with this mechanism, >75% of 125 At_{CAS}-RSPHERE and 106 At_{IS}-RSPHERE strains rescued *fro2* Fe deficiency symptoms at acidic pH, with ≥50% of strains in each represented bacterial class showing rescue, irrespective of parent soil origin (Figure S3C; Table S1), indicating that rescue of *fro2* Fe deficiency symptoms under acidic pH is widespread among *A. thaliana* root commensals.

Different coumarin structure types are required for bacterial rescue of host Fe deficiency under different pH

To identify coumarins required for IT466-mediated Fe deficiency rescue at different pH, we tested coumarin-biosynthesis-pathway mutants under unavFe conditions. Under acidic pH, double mutants of each coumarin-biosynthesis gene and *fro2* were used to test the *FRO2*-independent rescue activity.

Coumarin biosynthesis was required for IT466-mediated rescue of Fe deficiency and shoot Fe accumulation at both pH conditions, as neither *f6'h1* nor *fro2 f6'h1* mutants were rescued (Figures 2B and S4). However, the required coumarin differed with pH. At circumneutral pH, IT466 rescued *cyp82C4* but not *s8h* mutants, indicating that fraxetin—but not sideretin—is required for rescue, consistent with previous SynCom findings.[9] In contrast, at acidic pH, IT466 failed to rescue Fe deficiency in any *fro2* coumarin-biosynthesis double mutant, including *fro2 cyp82C4* (Figures 2B and S4B), indicating that sideretin is required for FRO2-independent Fe acquisition. Consistent with this, three different SynComs predominantly required sideretin to alleviate *fro2* Fe deficiency symptoms (Figures S5A–5C). Moreover, IT466 failed to fully rescue *cyp82C4* single-mutant plants, indicating that sideretin contributes to Fe deficiency rescue under acidic pH also when FRO2 is functional (Figure S4C).

Supporting the ecological relevance of our gnotobiotic experiments, *FRO2* was dispensable for plant growth and shoot chlorophyll accumulation in two natural soils with lower pH but essential in two circumneutral soils (Figures S6A–S6B). In contrast, *fro2 f6'h1* and *irt1* plants were strongly stunted and chlorotic across all soils, consistent with the strategy I requirement for Fe(II) uptake and highlighting the role of coumarin-dependent complementation of FRO2 function under natural, microbe-rich conditions at lower pH.

Figure 2. pH-specific enrichment patterns of coumarins in root exudates match coumarin chemotypes needed for bacterium-mediated rescue of plant Fe deficiency

(A) Shoot total chlorophyll concentration of *A. thaliana fro2* and *irt1* plants co-cultivated with heat-killed (hk) or live IT466 under unavFe (100 μM $FeCl_3$) at pH 7.4 (left) or pH 5.7 (right). Asterisks indicate significant differences between hk and live IT466 for each genotype (Kruskal-Wallis test followed by pairwise Wilcoxon tests with Benjamini-Hochberg correction; $^{*}p_{adj} < 0.05$, $^{**}p_{adj} < 0.01$, $^{***}p_{adj} < 0.001$, and $^{****}p_{adj} < 0.0001$; $n = 8$ (left) and $n = 6$–10 (right), two independent experiments.

(B) Shoot total chlorophyll of *A. thaliana* genotypes co-cultivated with hk or live IT466 under unavFe (100 μM $FeCl_3$) at pH 7.4 (left) or pH 5.7 (right). Different letters indicate significant differences among conditions (Kruskal-Wallis test followed by Dunn's post hoc test with Benjamini-Hochberg correction; $p_{adj} < 0.05$; $n = 14$–15 (left), two independent experiments; $n = 10$–17 (right), three independent experiments).

(C) Shoot total chlorophyll concentration of *A. thaliana* genotypes co-cultivated for 2 weeks with hk or live IT466 under unavFe (100 μM $FeCl_3$) at pH 7.4 (left) or pH 5.7 (right). Equimolar concentrations of the indicated compounds or solvent (1:1 water/DMSO; mock) were added at 100 μM (pH 7.4) or 50 μM (pH 5.7) to the growth medium. Asterisks indicate significant differences between hk and live IT466 for each treatment and genotype (Kruskal-Wallis test followed by pairwise Wilcoxon tests with Benjamini-Hochberg correction; $^{*}p_{adj} < 0.05$, $^{**}p_{adj} < 0.01$, $^{***}p_{adj} < 0.001$, and $^{****}p_{adj} < 0.0001$; $n = 8$–10 (left), two independent experiments; $n = 10$–17 (right), four independent experiments).

(D) Coumarin exudation rates from roots of the indicated *A. thaliana* genotypes under unavFe (100 μM $FeCl_3$) in axenic or live IT466 conditions. Asterisks indicate significant differences between pH conditions for each coumarin (Kruskal-Wallis test followed by pairwise Wilcoxon tests with Benjamini-Hochberg correction; $p_{adj} < 0.05$; $n = 6$, three independent experiments). The coumarin biosynthesis pathway is shown below, with coumarins enriched at each pH highlighted accordingly.

Please cite this article in press as: Malisic et al., *Arabidopsis* uses distinct coumarins and bacterial pathways for pH-adaptive iron acquisition, Cell (2026), https://doi.org/10.1016/j.cell.2026.09.030

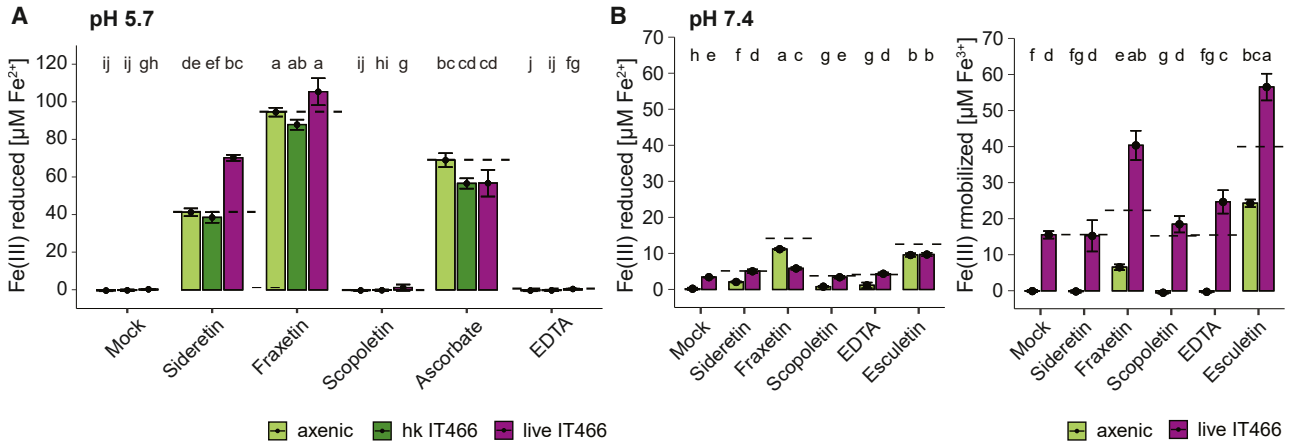

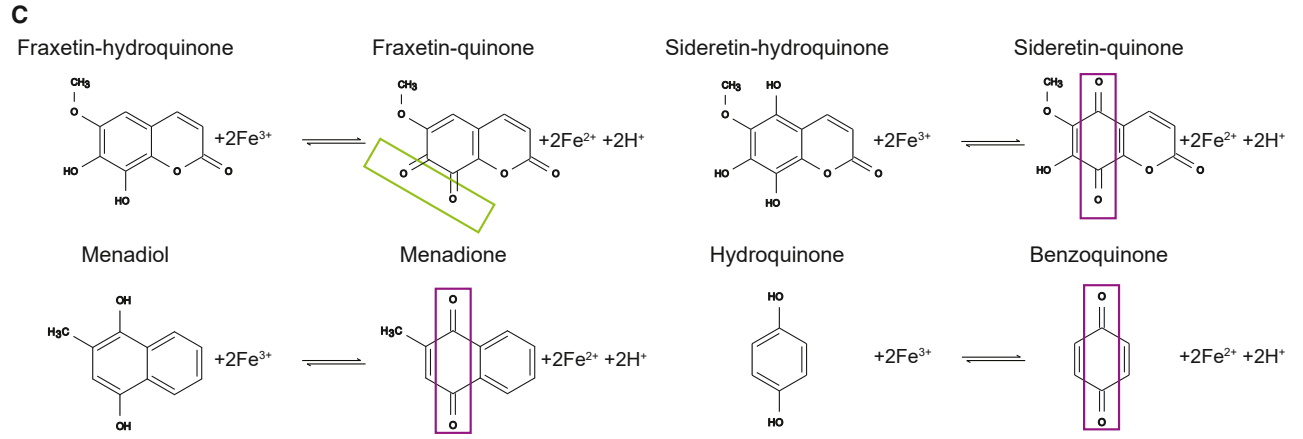

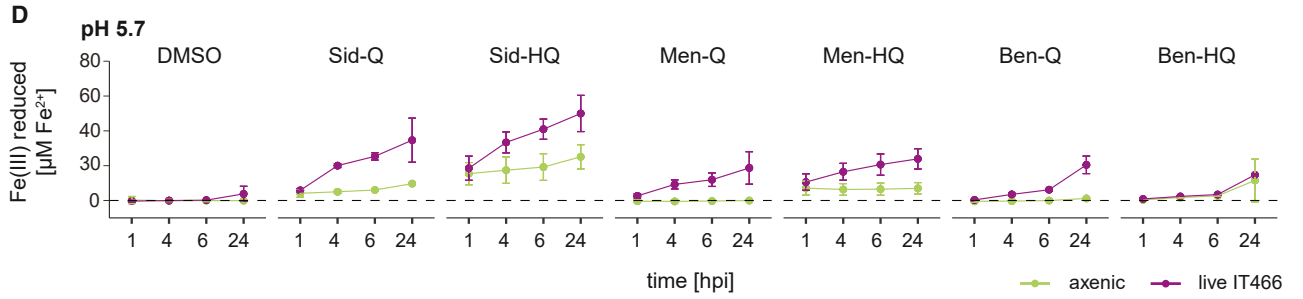

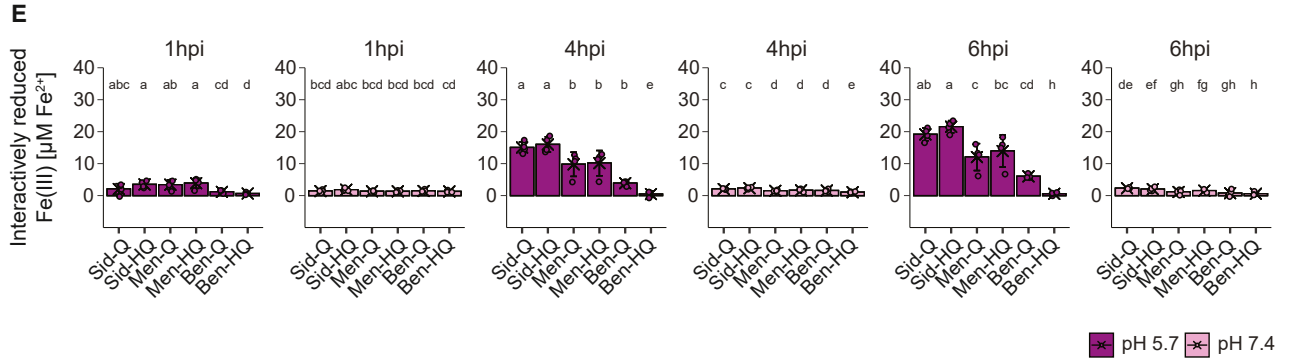

(legend on next page)

Please cite this article in press as: Malisic et al., *Arabidopsis* uses distinct coumarins and bacterial pathways for pH-adaptive iron acquisition, Cell (2026), https://doi.org/10.1016/j.cell.2026.09.030

At circumneutral pH, exogenous fraxetin or EDTA, but not scopoletin, sideretin or ascorbate, restored IT466-mediated rescue of *f6′h1* plants. This indicates that the distinctive and shared function of Fe(III) chelation of the former two molecules[30] underlies Fe-beneficial interactions with the bacterium under these conditions (Figure 2C).

Under acidic pH, fraxetin rescued Fe deficiency in germ-free *fro2 f6′h1* plants, but the rescue was reduced in the presence of IT466 (Figure 2C). This demonstrates that in the presence of the bacterium, fraxetin production is beneficial under circumneutral pH but less so under acidic pH. In contrast, sideretin supplementation at acidic pH led to synergistic effects with IT466, fully rescuing the Fe-deficiency phenotype with respect to shoot biomass and chlorophyll concentrations, as sideretin or IT466 treatment alone did not improve these host performance parameters (Figure 2C). The failure of EDTA to rescue *fro2 f6′h1* with IT466, together with the absence of sideretin-dependent rescue in *irt1*, indicates that Fe(III) reduction and subsequent Fe(II) uptake, rather than chelation, underlie IT466-mediated Fe acquisition at acidic pH (Figure 2C).

Bacterial interactions with fraxetin at circumneutral pH and sideretin at acidic pH aligned with the pH-dependent coumarin exudation patterns of WT and *fro2* plants under unavFe conditions (Figure 2D). Overall, coumarin exudation increased under unavFe compared with avFe, indicating activation of the Fe-deficiency program in the presence of immobile Fe (Figure S7A). Fraxetin was enriched at circumneutral pH and depleted at acidic pH, whereas the inverse pattern was observed for sideretin (Figure 2D). Scopoletin and esculetin were also depleted at pH 5.7, suggesting redirection of metabolic flux toward sideretin biosynthesis under acidic conditions, consistent with previous reports.[30,40,44,45] Importantly, IT466 did not affect sideretin or fraxetin exudation rates at either pH (Figure 2D). In addition, coumarin biosynthesis did not substantially alter IT466's root colonization capacity (Figure S3D). Similar to IT466-colonized plants, coumarin exudation rates of WT plants co-cultured with taxonomically diverse root microbiota members were unaffected (Figure S7B).

Together, these results suggest that pH-dependent coumarin exudation is a host-autonomous process associated with distinct functional interactions between plants and root-associated bacteria for Fe mobilization, involving Fe(III) chelation at circumneutral pH and Fe(III) reduction at acidic pH.

Ex planta coumarin-commensal interactions for Fe mobilization

To characterize the interaction between IT466 and coumarins, we measured Fe(III) reduction *ex planta*, where IT466 and coumarins were incubated with $FeCl_3$ in the presence of ferrozine, which mimics the root environment as an Fe(II) sink.

As expected, the known reductant ascorbate reduced Fe(III), whereas the Fe(III)-chelating agent EDTA and the coumarin scopoletin did not (Figures 3A and S8A). Sideretin and fraxetin showed pH-dependent Fe(III) reduction, with greater activity at pH 5.7 than at pH 7.4 (Figure S8A), consistent with previous reports.[30,34] IT466 alone did not reduce Fe(III) but synergized with sideretin at pH 5.7, increasing Fe(III) reduction beyond the summed activity of either component alone (Figures 3A and S8A). This interaction was absent with fraxetin, consistent with the inability of IT466 to rescue *fro2 cyp82C4* at acidic pH (Figures 2B and S4B). Similar sideretin-dependent synergy was observed with the three SynComs (Figure S8B). Lack of interactions for Fe(III) reduction between all tested coumarins and IT466 at pH 7.4 is consistent with the failure of IT466 to alleviate *fro2* Fe deficiency at circumneutral pH (Figures 2A and S8A).

Bacterial siderophores, such as PVD, predicted to be produced by IT466, are high-affinity Fe(III) chelators believed to contribute to plant Fe nutrition and are secreted under Fe-limiting conditions.[56–60] To assess potential siderophore-dependent interactions, we tested supernatants from Fe-limited IT466 cultures for Fe mobilization under circumneutral pH. Abiotic Fe mobilization was not observed for EDTA, sideretin, or scopoletin, but for fraxetin and esculetin (Figures 3B and S8C). Similarly, IT466 supernatants mobilized Fe, predominantly as Fe(III), and synergized with Fe(III)-chelating coumarins to increase Fe(III), but not Fe(II), mobilization (Figures 3B and S8C). Consistent with the *FRO2*- and fraxetin-biosynthesis requirement for IT466-mediated rescue of plant Fe deficiency at circumneutral pH (Figures 3B, 2A–2C, and S4A), this interaction occurred with fraxetin but not scopoletin or sideretin.

Together, these results show that sideretin interacts with IT466 or SynComs to mobilize Fe via reductive dissolution at acidic pH, while fraxetin interacts with IT466 for Fe(III) mobilization via chelation under circumneutral conditions. These pH-specific modes of interactive Fe mobilization—reduction versus chelation—mirror the differential *FRO2* requirement for microbe-mediated rescue of host Fe starvation observed under contrasting pH conditions (Figure 2). Moreover, a general Fe(III)-chelating function of

Figure 3. pH-specific coumarin structure types are needed for IT466-mediated Fe mobilization *ex planta*

(A) Fe(III) reduction by 50 μM of the indicated compounds in the presence of hk or live IT466 (OD_{600} = 0.1), or without bacteria (axenic), under unavFe (100 μM $FeCl_3$) at pH 5.7 after 24 h. Dashed lines indicate the sum of abiotic and IT466-mediated Fe mobilization. Data are mean ± SD. Different letters indicate significant differences (Kruskal-Wallis test followed by pairwise Wilcoxon tests with Benjamini-Hochberg correction; $p_{adj} < 0.05$; $n = 4$, two independent experiments).

(B) Fe mobilization from unavFe (100 μM $FeCl_3$) by Fe-limited IT466 culture supernatants in the presence of 100 μM of the indicated compounds at pH 7.4 after 6 h. Data are mean ± SD. Different letters indicate significant differences (Kruskal-Wallis test followed by pairwise Wilcoxon tests with Benjamini-Hochberg correction; $p_{adj} < 0.05$; $n = 3$). The dashed lines depict the sum of abiotically mobilized Fe plus Fe mobilized by IT466 supernatants (left: Fe(II), right: Fe(III)).

(C) Proton-coupled Fe(III) reduction by sideretin, fraxetin, menadiol, and *p*-hydroquinone. Chemical structures of the reduced and expected oxidized forms generated upon Fe(III) reduction are displayed.

(D) Time-dependent *in vitro* Fe(III) reduction from 100 μM $FeCl_3$ by 50 μM of the indicated redox-active compounds in the presence (live IT466) or without bacteria (axenic). Data are mean ± SD ($n = 4$, three independent experiments).

(E) Interactive Fe(III) reduction from unavFe (100 μM $FeCl_3$) by each indicated compound after 1, 4, and 6 h of incubation at pH 5.7 or 7.4. Data are extracted from (D). Error bars indicate ± SD. Different letters indicate significant differences between treatments and pH conditions at each time point (Kruskal-Wallis test followed by pairwise Wilcoxon tests with Benjamini-Hochberg correction; $p_{adj} < 0.05$; $n = 4$, three independent experiments).

Please cite this article in press as: Malisic et al., *Arabidopsis* uses distinct coumarins and bacterial pathways for pH-adaptive iron acquisition, Cell (2026), https://doi.org/10.1016/j.cell.2026.09.030

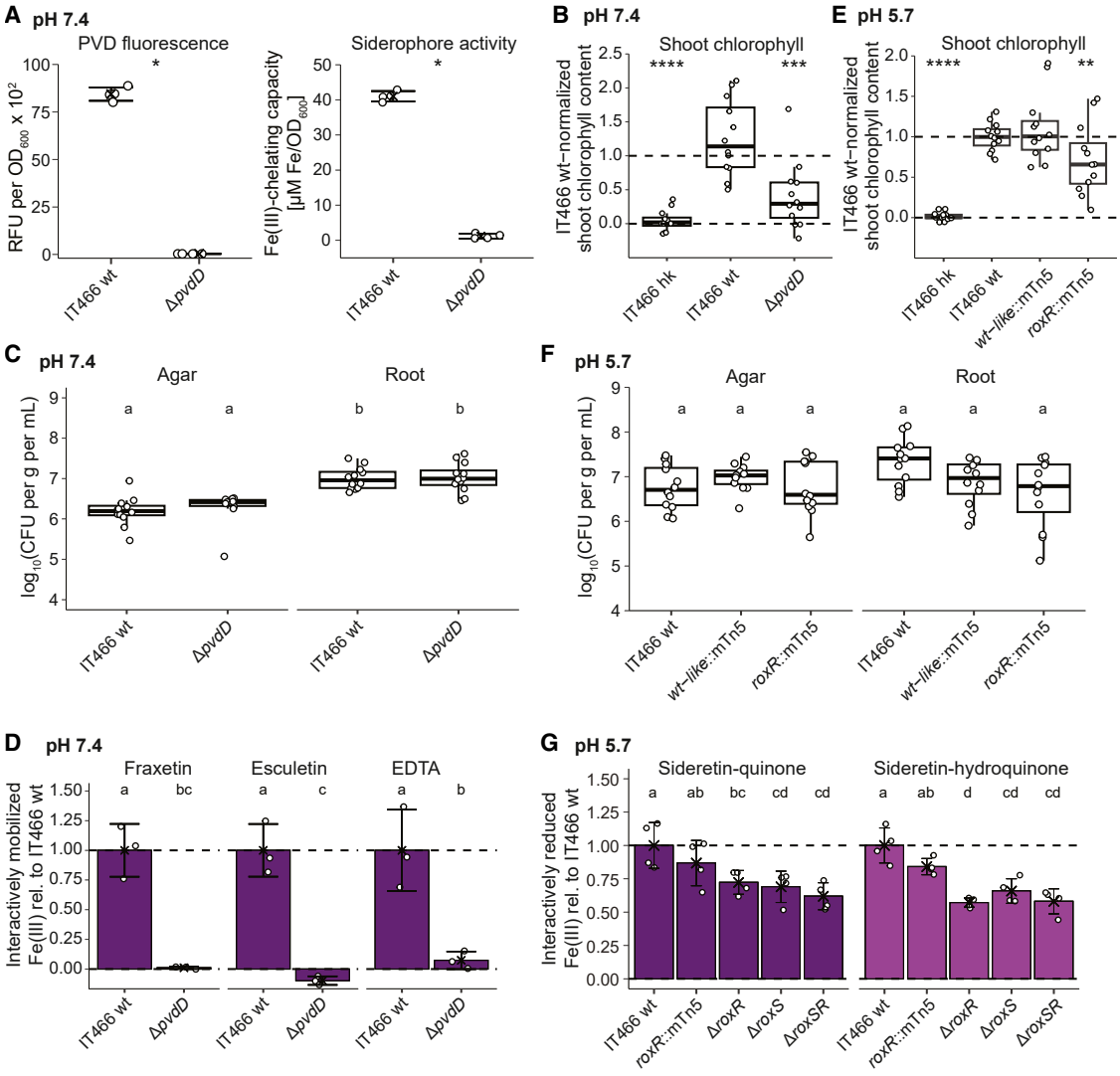

Figure 4. pH-specific coumarin exometabolites engage different bacterial mechanisms to alleviate plant Fe deficiency

(A) Relative fluorescence units (RFUs) normalized to OD_{600} (left) and Fe(III)-chelating capacity (right) of Fe-limited culture supernatants of IT466 WT or Δ*pvdD*. Data are mean ± SD. Asterisks indicate significant differences from IT466 WT (Kruskal-Wallis test followed by pairwise Wilcoxon tests; *$p < 0.05$, **$p < 0.01$, ***$p < 0.001$, and ****$p < 0.0001$; $n = 4$).

(B) Shoot total chlorophyll concentrations of *A. thaliana* WT plants co-cultivated for 2 weeks with hk IT466 WT or the indicated genotypes with 100 µM $FeCl_3$ at pH 7.4. Values are normalized such that IT466 WT is 1 and IT466 hk is 0 (dashed lines). Asterisks indicate significant differences from IT466 WT (Kruskal-Wallis test followed by pairwise Wilcoxon test; *$p_{adj} < 0.05$, **$p_{adj} < 0.01$, ***$p_{adj} < 0.001$, and ****$p_{adj} < 0.0001$; $n = 12$, four independent experiments).

(C) Bacterial titers of IT466 WT or Δ*pvdD* on *A. thaliana* WT roots or in agar compartment after 2 weeks of co-cultivation (initial $OD_{600} = 0.0001$) with 100 µM $FeCl_3$ at pH 7.4. Different letters indicate significant differences (Kruskal-Wallis test with Dunn's post hoc test and Benjamini-Hochberg correction, $p_{adj} < 0.05$; $n = 12$, four independent experiments).

(D) Interactive Fe(III) mobilization from 100 µM $FeCl_3$ by Fe-limited culture supernatants of IT466 genotypes in the presence of the indicated compounds (100 µM) at pH 7.4 after 6 h. Values were calculated by subtracting Fe(III) mobilized by the supernatant and compound individually from combined-treatment values and normalized to IT466 WT supernatant (100%) and medium control (0%). Crossbars indicate mean ± SD. Different letters indicate significant differences (Kruskal-Wallis test followed by pairwise Wilcoxon tests with Benjamini-Hochberg correction, $p_{adj} < 0.05$; $n = 3$).

(E) Shoot chlorophyll concentrations of *A. thaliana fro2* plants co-cultivated for 2 weeks with hk IT466 WT or the indicated genotypes with 100 µM $FeCl_3$ at pH 5.7. Values are normalized such that IT466 WT is 1 and IT466 hk is 0 (dashed lines). Asterisks indicate significant differences from IT466 WT (Kruskal-Wallis test followed by pairwise Wilcoxon tests with Benjamini-Hochberg correction; *$p_{adj} < 0.05$, **$p_{adj} < 0.01$, ***$p_{adj} < 0.001$, and ****$p_{adj} < 0.0001$; $n = 12$–16, four independent experiments).

(legend continued on next page)

Please cite this article in press as: Malisic et al., *Arabidopsis* uses distinct coumarins and bacterial pathways for pH-adaptive iron acquisition, Cell (2026), https://doi.org/10.1016/j.cell.2026.09.030

coumarins appears to be sufficient to drive interactive Fe mobilization with IT466 at circumneutral pH, as fraxetin could be functionally replaced by the synthetic Fe(III)-chelator EDTA. Conversely, at acidic pH, sideretin could not be functionally replaced by other Fe(III)-reducing molecules such as ascorbate (Figure 3A), implying that a particular structural moiety in sideretin is needed for interactive Fe(III) reduction with IT466.

The *p*-quinone moiety defines the specificity of synergistic sideretin-IT466 interactions under acidic conditions

We next sought to determine functional groups underlying sideretin-IT466 interactions for Fe(III) reduction under acidic conditions. In its reduced form (hydroquinone-type), sideretin differs from fraxetin by an additional hydroxyl group, forming a *para*-dihydroxy arrangement that is thought to be primarily responsible for the Fe(III)-reducing activity of sideretin, whereas Fe(III) reduction by fraxetin is mediated by the *ortho*-dihydroxy moiety (Figure 3C).[30,34] Proton-coupled 2Fe(III) reduction through the hydroxyl groups yields the oxidized (quinone-type) forms of these coumarins (Figure 3C).[34]

To test whether the *p*-(hydro)quinone motif is sufficient for synergistic Fe(III) reduction with IT466, we tested additional *p*-hydroquinone/*p*-quinone pairs, menadiol/menadione, and hydroquinone/benzoquinone, alongside sideretin/palladium-air-oxidized sideretin (for simplicity referred to as sideretin-hydroquinone/sideretin-quinone) at acidic pH. Sideretin-hydroquinone showed the highest abiotic Fe(III) reduction, followed by menadiol and *p*-hydroquinone, whereas the oxidized forms exhibited little to no abiotic activity (Figure 3D). In the absence of quinone molecules, Fe(III) reduction by IT466 was negligible (Figure 3D). In contrast, both reduced and oxidized *p*-quinones synergized with IT466 to promote Fe(III) reduction, with sideretin showing the strongest interaction, followed by menadione and benzoquinone (Figures 3D and 3E). No such synergy occurred at pH 7.4, indicating that IT466-mediated Fe(III) reduction with *p*-quinones is strongly pH dependent (Figure 3E).

Together, these results demonstrate that *p*-quinones are sufficient for interactive Fe(III) reduction with IT466 under acidic conditions, with the quinone/hydroquinone identity defining the magnitude of the interaction. The fact that IT466 interacts synergistically for Fe(III) reduction with compounds sharing similar redox-active structural features suggests that the genetic determinants in IT466 underlying the interactions are at least partially conserved across structurally diverse *p*-quinones.

pH-specific coumarins engage distinct microbial mechanisms for Fe mobilization to alleviate plant Fe deficiency

To dissect how IT466 promotes synergistic Fe mobilization with coumarins, we used reverse and forward genetics. We first targeted the *Pseudomonas* siderophore PVD, which mobilizes Fe(III) under Fe limitation and can promote Fe nutrition in *A. thaliana* when supplied as a purified compound.[61–63] We generated a chromosomal *pvdD* deletion in IT466 (Δ*pvdD*), encoding a non-ribosomal peptide synthetase predicted to be required for intact PVD biosynthesis,[64] which eliminated PVD production, as confirmed by loss of PVD-associated fluorescence and Fe(III)-chelating activity in Fe-limited culture supernatants (Figure 4A). At circumneutral pH, Δ*pvdD* retained WT-like root colonization but showed reduced rescue of Fe-deficient plants, without affecting plant performance under avFe (Figures 4B, 4C, S9A, and S9B). Consistently, Δ*pvdD* supernatants failed to mobilize Fe(III), either alone or synergistically with fraxetin, esculetin, or EDTA *ex planta* (Figures 4D and S9C). By contrast, *pvdD* was dispensable for IT466-mediated rescue under acidic conditions (Figures S9D and S9E). Together, these results suggest that PVD is needed for interactive Fe(III) mobilization with fraxetin and the rescue of host Fe deficiency, specifically at circumneutral pH.

To identify bacterial determinants mediating synergistic Fe(III) reduction between IT466 and sideretin under acidic pH, we generated an *mTn5* insertion library and screened for mutants defective in menadione-dependent Fe(III) reduction, using menadione as a functional surrogate for sideretin. We adapted the liquid ferrozine assay to an agar-based format, enabling visual detection of Fe(II) formation as a pink ferrozine-Fe(II) halo around individual colonies (Figures 3C–3E and S10A). Of the ~4,000 mutants screened, 40 candidates were validated, representing 17 insertion sites across 12 genes (Figure S10B; Table S2). We identified only one mutant, containing an insertion in the redox-sensing-associated gene *roxR* (*roxR*::*mTn5*),[48,65,66] with impaired rescue despite WT-like root and agar colonization (Figures 4E, 4F, S10C, and S10D). This defect was specific to unavFe conditions and acidic pH, as *roxR*::*mTn5* did not differ from IT466 WT under avFe or under unavFe at circumneutral pH (Figure S11).

RoxR functions as the response regulator of the redox-sensing two-component system RoxSR, which acts together with the sensor kinase RoxS in homologous systems such as RegBA (*Rhodobacter capsulatus*) and PrrBA (*Rhodobacter sphaeroides*).[48,49,67] To validate the role of RoxSR, we generated Δ*roxR*, Δ*roxS*, and Δ*roxSR* mutants. Unlike *roxR*::*mTn5*, all three deletion mutants failed to colonize roots and the agar compartment, indicating that complete disruption of RoxSR compromises bacterial proliferation in the assay and that *roxR*::*mTn5* may retain residual RoxR activity (Figures S12A and S12B).

To further characterize the mutants in an *ex planta* assay in which growth differences can be neglected, we examined the ability of *roxR*::mTn5, Δ*roxR*, Δ*roxS*, and Δ*roxSR* to synergistically reduce Fe(III) with sideretin in the liquid ferrozine assay. Strains were pre-cultivated in a nutrient-rich medium, where all

(F) Bacterial titers of IT466 genotypes on *A. thaliana fro2* roots or in the agar compartment after 2 weeks of co-cultivation with 100 μM $FeCl_3$ at pH 5.7 (initial OD_{600} = 0.0001). Different letters indicate significant differences (Kruskal-Wallis test with Dunn's post hoc test and Benjamini-Hochberg correction; $p_{adj} < 0.05$); n = 12–16, three independent experiments.

(G) Interactive Fe(III) reduction from 100 μM $FeCl_3$ by *roxSR*-related IT466 mutants relative to IT466 WT in the presence of 50 μM sideretin-quinone or sideretin-hydroquinone at pH 5.7 after 4 h. Fe(II) was quantified using the ferrozine assay. Crossbars indicate mean ± SD. Different letters indicate significant differences (Kruskal-Wallis test followed by pairwise Wilcoxon tests with Benjamini-Hochberg correction; $p_{adj} < 0.05$; n = 4, four independent experiments).

Please cite this article in press as: Malisic et al., *Arabidopsis* uses distinct coumarins and bacterial pathways for pH-adaptive iron acquisition, Cell (2026), https://doi.org/10.1016/j.cell.2026.09.030

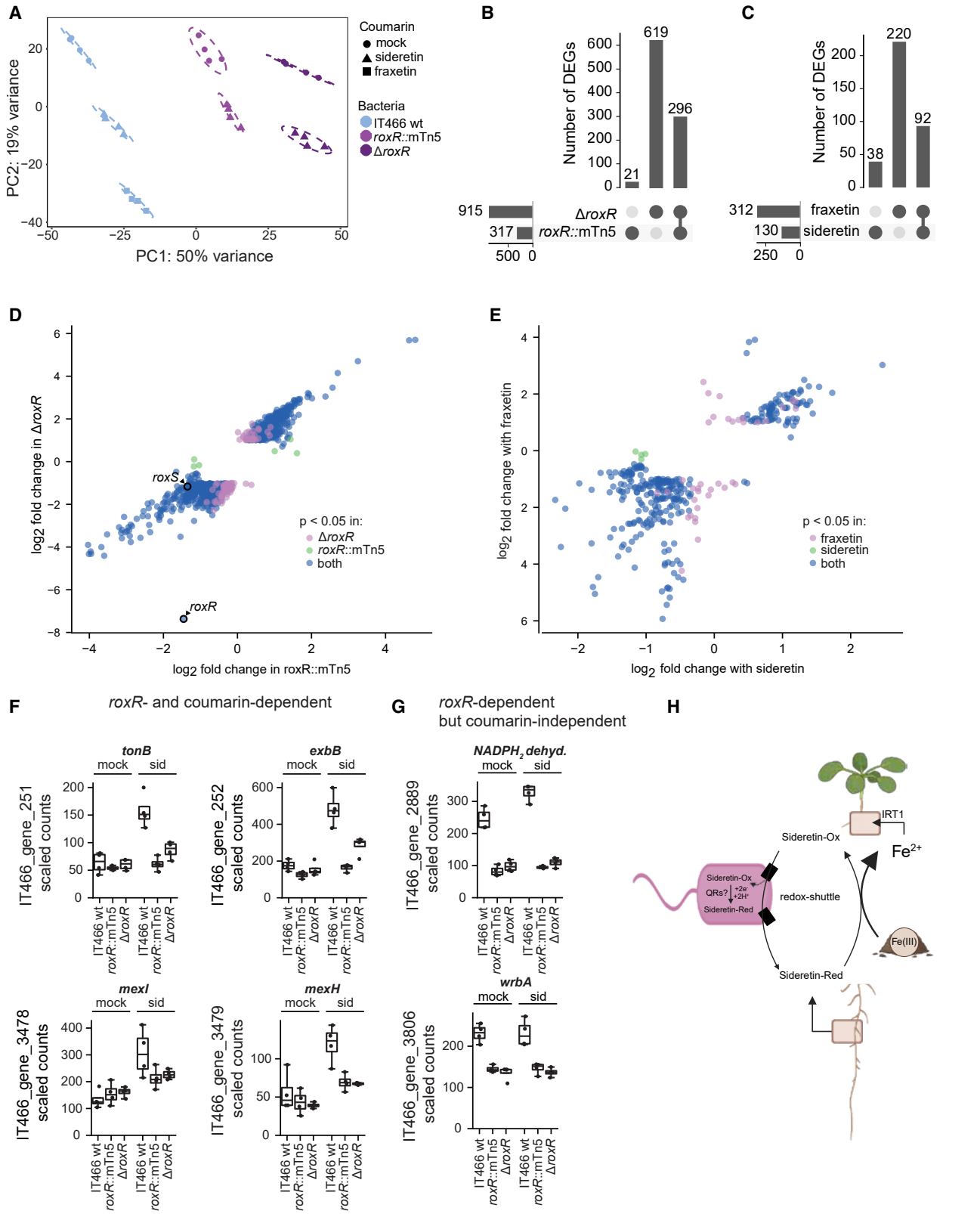

(legend on next page)

Please cite this article in press as: Malisic et al., *Arabidopsis* uses distinct coumarins and bacterial pathways for pH-adaptive iron acquisition, Cell (2026), https://doi.org/10.1016/j.cell.2026.09.030

bacterial genotypes exhibited comparable growth after 48 h of cultivation, the time point at which cells were harvested for the ferrozine assay (Figures S12C and S12D). All bacterial genotypes were then inoculated into the assay medium at OD_{600} = 0.1, allowing for a comparison of their Fe reducing activities. *roxR*::*mTn5* showed reduced synergistic Fe(III) reduction with sideretin, whereas Δ*roxR* exhibited a stronger defect; Δ*roxS* and Δ*roxSR* phenocopied Δ*roxR*, demonstrating that the RoxSR two-component system is required for sideretin-dependent Fe(III) reduction by IT466 (Figure 4G). RoxSR mutants were similarly impaired in interactions with menadione but not with menadiol (Figure S12E). Together with the ability of *p*-quinones to drive interactive Fe(III) reduction with IT466 (Figures 3D and 3E), these results implicate the oxidized *p*-quinone form of sideretin as the relevant chemotype for RoxSR-dependent Fe(III) reduction. Thus, RoxSR-mediated interactions between IT466 and sideretin are required for Fe(III) reduction and the rescue of the *fro2* Fe-deficiency phenotype, specifically under acidic pH.

RoxR-dependent IT466 transcripts comprise sideretin-responsive and non-responsive genes

To determine how *roxR* mediates synergistic Fe(III) reduction with sideretin, we performed RNA sequencing (RNA-seq) under the conditions used for the *ex planta* Fe(III) reduction assay (pH 5.7, 100 μM $FeCl_3$, ferrozine). *roxR* transcript was absent in Δ*roxR*, whereas *roxR*::*mTn5* retained 37% of WT transcript abundance, with the deduced amino acid sequence lacking the first 27 amino acid residues from the N terminus (Tables S3–S5; Figure S13A). Across the two *roxR* mutants, 936 genes were differentially expressed relative to WT, with qualitatively similar expression patterns but fewer differentially expressed genes (DEGs) in *roxR*::*mTn5*, consistent with its residual *roxR* expression (Figures 5A, 5B, and 5D). WT IT466 also mounted a substantial transcriptional response to both sideretin and fraxetin, with extensive overlap between the two coumarins, indicating a shared transcriptional response (Figures 5A, 5C, and 5E).

Functional enrichment of DEGs revealed RoxR- and coumarin-dependent changes in energy metabolism, including denitrification, as well as Fe transport and homeostasis (Figure S13B). Siderophore biosynthesis genes were among the affected transcripts, but these changes are unlikely to account for the sideretin-IT466 Fe(III)-reduction phenotype because *roxR* disruption and coumarin treatment produced similar transcriptional responses in these genes, whereas only *roxR* disruption impaired the interaction (Figures 4E and 4G). Further, *pvdD* was dispensable for IT466-mediated rescue under acidic pH (Figure S9D).

We next identified genes showing a *roxR*-dependent response to coumarins. Four of the 61 candidates—*tonB*, *exbB*, *mexH*, and *mexI*—were strongly induced by sideretin in a RoxR-dependent manner and showed similar responses to fraxetin (Figures 5F, S13C, and S13D), consistent with the roles of their homologs in the transport of plant-derived redox-active compounds.[68–71] We also identified *roxR*-dependent redox enzymes whose expression was not altered by coumarins, including flavin-dependent quinone oxidoreductases previously shown to reduce menadione and/or *p*-benzoquinone (Figure 5G).[72,73] Together, these candidates suggest that RoxR may promote sideretin-dependent Fe(III) reduction through coordinated coumarin transport and intracellular quinone reduction (Figure 5H).

Bacteria contain other redox-sensing systems, with distinct oxygen-sensing mechanisms but partially overlapping downstream targets compared to RoxR, such as the transcriptional regulator Anr, termed Fnr in *Escherichia coli*.[65,74] We therefore tested its contribution to IT466-mediated Fe deficiency rescue. Δ*anr* showed a rescue defect comparable to *roxR*::*mTn5* despite WT-like root colonization (Figures S14A and S14B). Both RoxSR and Anr are regulators of bacterial respiratory metabolism in response to environmental oxygen conditions.[65,66,75] To rule out that the defects in host Fe deficiency rescue by the *roxR*::*mTn5* and Δ*anr* mutants are due to general perturbations in oxygen metabolism, we generated a chromosomal deletion mutant in the *petCBA* operon and an independent deletion mutant in *cco-1/cco-2*, which encode components of the cytochrome bc1 and cytochrome c oxidase complexes, respectively.[75–78] Compared with the WT IT466 strain, the growth defects of the Δ*petCBA* and Δ*cco-1* Δ*cco-2* mutants were

Figure 5. Sideretin-driven Fe(III) reduction by IT466 may involve RoxR-dependent components that include both sideretin-responsive and sideretin-unresponsive elements

(A) Principal component analysis of *ex planta* IT466 WT, *roxR*::mTn5, and Δ*roxR* transcriptomes under sideretin, fraxetin (50 μM each), or mock treatment at pH 5.7 and unavFe (100 μM $FeCl_3$). Colors indicate IT466 genotypes, and shapes indicate treatments. n = 4 biological replicates.

(B) Upset plot showing genes differentially expressed in *roxR*::mTn5 or Δ*roxR*, compared with IT466 WT without coumarin treatment. DEGs are defined by $\log_2$ fold change ($\log_2$FC) > +1 or $\log_2$FC < −1 and $p_{adj} < 0.05$.

(C) Upset plot showing genes with differential expression in IT466 WT treated with sideretin or fraxetin, compared with mock. DEGs are defined by $\log_2$FC > +1 or $\log_2$FC < −1 and $p_{adj} < 0.05$.

(D) $\log_2$FC of genes differentially expressed in at least one mutant strain, compared to IT466 WT, in the absence of coumarins. *roxR* and *roxS* are outlined in black and marked with black arrowheads. Point color indicates significance ($p_{adj} \leq 0.05$) in each mutant.

(E) $\log_2$FC of genes differentially expressed in IT466 WT in at least one coumarin treatment, compared with mock conditions. Point color indicates significance ($p_{adj} \leq 0.05$) within each treatment.

(F) Expression levels of genes forming a candidate coumarin import-export module that underly *roxR*-dependent induction by coumarins. *tonB*, *exbB* (import candidates), and *mexH*, *mexI* (export candidates).

(G) Expression of candidate *roxR*-dependent, coumarin-unresponsive genes potentially mediating intracellular reduction of sideretin-quinone to sideretin-hydroquinone.

(H) Proposed sideretin redox-shuttle model. Root-derived sideretin reduces Fe(III) extracellularly and is oxidized to sideretin-quinone. The quinone may be imported through a RoxR-dependent TonB/ExbB system, reduced intracellularly by candidate flavin mononucleotide-dependent quinone oxidoreductases, and exported through a MexH/MexI system for subsequent Fe(III) reduction. Transport genes are sideretin responsive, whereas candidate reductases are RoxR dependent but sideretin unresponsive.

Please cite this article in press as: Malisic et al., *Arabidopsis* uses distinct coumarins and bacterial pathways for pH-adaptive iron acquisition, Cell (2026), https://doi.org/10.1016/j.cell.2026.09.030

similar to those of the *roxSR*-related mutants and Δ*anr* mutants under low-oxygen conditions (microoxic and near-anoxic; Figure S14C). The Δ*petCBA* and Δ*cco-1* Δ*cco-2* mutants showed IT466 WT-like rescue of *fro2* Fe deficiency symptoms, suggesting that metabolic limitations under low oxygen are unlikely to explain the observed *in planta* phenotypes of *roxR*::*mTn5* and Δ*anr* (Figures S14A–S14C). RoxSR and Anr are also widespread among root-associated bacteria from At_{CAS}-RSPHERE and At_{IS}-RSPHERE (Figure S14D). Together, these findings suggest that root-exuded sideretin engages conserved bacterial redox-sensing pathways to promote Fe(III) reduction and alleviate host Fe deficiency.

DISCUSSION

Our study advances the understanding of plant-microbe interactions in micronutrient acquisition in several ways. First, by leveraging root microbiota culture collections from soils with different Fe bioavailability and pH, we show that microbial rescue of host Fe starvation across environmental pH is a widespread feature of bacterial root commensals and thus ubiquitous rather than a soil-specific adaptation (Figures 1 and S1). The "cry-for-help" hypothesis posits that stress-induced changes in root exudation result in the recruitment of specific microbial taxa to alleviate the host's stress.[19,79–81] As the rescue of plant Fe deficiency is such a prevalent and taxonomically widespread trait within microbial communities even from Fe-sufficient soil (Figures 1, S1, and S6), our data suggest an extension of the "cry-for-help" hypothesis; here, Fe-limitation-induced coumarin exudation stimulates a conserved activity of root-associated bacteria, leading to the rescue of plant symptoms via a functional but not necessarily a compositional change in the root microbial community.

Experiments with *Pseudomonas* IT466 in mono-association and with multiple SynComs demonstrate that this coumarin-dependent trait scales across diverse bacterial consortia (Figures 2, S3, and S5; Harbort et al.[9,51]). We reveal that microbiota-mediated plant Fe nutrition relies on two distinct mechanisms depending on the external pH and the corresponding coumarin chemotypes exuded by roots: interactive Fe(III) mobilization under circumneutral conditions and reductive dissolution of Fe(III) under acidic conditions. Consequently, FRO2 is dispensable for plant Fe acquisition under acidic conditions and can be functionally replaced by bacteria-coumarin interactions. Fe(II) import via IRT1, however, remains essential for Fe acquisition across pH. These findings extend the model of host-autonomous reductive Fe uptake converging on IRT1 in strategy I plants.[26,30] Our natural soil experiments support the ecological relevance of the mechanistic dichotomy uncovered using gnotobiotic plant growth systems (Figure S6).

Second, we dissected the molecular interplay between root-exuded coumarins and microbes, identifying microbial processes required for the rescue of plant Fe deficiency at different pH. At circumneutral pH, fraxetin interacts with IT466 to facilitate Fe(III) mobilization dependent on the biosynthesis of the *Pseudomonas* siderophore PVD. Since bacterial siderophores have been described in at least 20 bacterial genera and assigned to 4 different chemical classes, they might play a broad role in the bacterial root microbiota for Fe mobilization at near-neutral pH.[82] This does not preclude further functions of siderophores in intermicrobial competition, root microbiota establishment, and virulence for certain pathogens.[56,83,84] At acidic pH, by contrast, sideretin engages conserved bacterial redox-sensing systems (RoxSR and Anr) to promote reductive dissolution of Fe(III) (Figures 4 and S14). Residual host rescue activity observed for each mutant at each tested pH suggests the presence of additional mechanisms operating in IT466. Although IT466 and the other commensals tested did not alter coumarin exudation, some microbiota members may improve host Fe status by modulating root-exuded coumarins, as specific commensals have been shown to increase root coumarin content.[54,85]

Third, our *ex-planta* Fe mobilization experiments showed that the interactions between coumarins and commensals do not require a reciprocal dialog with the host (Figures 3, 4, and S8). This contrasts with the symbiotic relationships of legumes with dinitrogen-fixing rhizobia, where host-exuded (iso)flavonoids are first perceived by the bacteria, which then release Nod-factor signaling molecules that are perceived by specific plant receptors.[13,86,87] Instead, plants require only their own Fe uptake machinery, converging on IRT1, to scavenge the Fe mobilized through coumarin-microbe interactions. As Fe-limitation-induced coumarin exudation by roots and reductive import of Fe are widely observed in strategy I plant species,[34] our findings are likely applicable beyond *A. thaliana*. Given that siderophore production and redox sensing via RoxSR and Anr homologs are prevalent among diverse bacterial taxa (Figure S14D),[46–49] this could explain how a taxonomically broad range of microbiota members can alleviate host Fe starvation, compared with the taxonomically restricted symbiotic relationships with dinitrogen-fixing rhizobia or Glomeromycota (arbuscular mycorrhizal fungi).

At circumneutral pH, both siderophores and fraxetin can act as Fe mobilizers alone (Figures 3B, S8C, and S9C). Additionally, both compounds together can synergistically mobilize Fe(III) *ex planta* at this pH condition (Figures 3B, S8C, and S9C). The mechanism underlying cooperative Fe(III) mobilization by the commensal is yet to be determined, but siderophores have been shown to transform slowly diffusing large insoluble Fe(III) particles to small, quickly diffusing iron–siderophore complexes.[88] Plant Fe nutrition cannot directly benefit from bacterial siderophores, as evidenced by the inability of siderophore-producing IT466 to rescue Fe deficiency symptoms in fraxetin-deficient plants (Figure 2B). However, abiotic and biotic dissolution of Fe(III)-loaded siderophore complexes through hydrolysis and/or oxidation could facilitate Fe(III) ligand exchange with fraxetin. As fraxetin can be functionally replaced by the synthetic Fe(III)-chelator EDTA in interactions with IT466 (Figure 2C), whose Fe-chelated form [Fe(III)–EDTA] serves as a well-characterized substrate of the ferric-chelate reductase FRO2,[30] we propose that *in planta* synergistic Fe mobilization involves fraxetin as an Fe(III) shuttle. This fraxetin-Fe(III) shuttle would link bacterial siderophore-mediated Fe(III) mobilization with reductive uptake via the FRO2–IRT1 module for sustained Fe(III) mobilization from insoluble Fe precipitates. The proposed mechanism could operate with structurally diverse siderophores produced by various groups of microbes,[46,58,82] consistent with the observed

Please cite this article in press as: Malisic et al., *Arabidopsis* uses distinct coumarins and bacterial pathways for pH-adaptive iron acquisition, Cell (2026), https://doi.org/10.1016/j.cell.2026.09.030

taxonomically widespread rescue of host Fe deficiency at circumneutral pH and supported by recent work implicating a structurally distinct *Bacillus* siderophore in *A. thaliana* Fe nutrition.[57] Whether some Fe-loaded siderophores can also act as direct FRO2 substrates remains to be tested.

Under acidic pH, we hypothesize that the RoxSR two-component system controls a redox shuttle required for Fe(III) reduction. In this scenario, extracellular sideretin quinone is imported into bacteria, reduced to sideretin hydroquinone, and re-exported for extracellular Fe(III) reduction (Figure 5H). This mechanism could link sideretin recycling to bacterial quinone homeostasis, in which intracellular quinone reductases reduce redox-active quinones and limit oxidative stress.[89,90] This model is supported by transcriptomic analysis of IT466, which identified sideretin-mediated induction of RoxR-dependent expression of genes with roles in redox reactions and transport of redox-active metabolites: *tonB* and *exbB* homologs, which are implicated in Fe(III)-chelate and plant-derived catechol import,[70,71] as well as the RND family transporters *mexH* and *mexI*,[69,91] whose homologs transcriptionally respond to and export redox-active metabolites (Figure 5F). Because fraxetin elicited a similar transcriptional response, the sideretin specificity of the redox phenotype may instead be derived from a coumarin-independent, RoxR-dependent set of genes, including conserved flavin- and NAD(P)H-dependent quinone oxidoreductases such as the NQO1-like WrbA enzyme (Figure 5G).[89,90,92,93] The higher redox potential of coumarins compared with reduced flavins—which serve as a non-covalently bound prosthetic group to catalyze the reaction of these bacterial enzymes—is compatible with this model. Furthermore, the substrate promiscuity of these oxidoreductase families, which reduce planar quinones and can accommodate coumarin derivatives,[89,93,94] is concordant with the ability of the naphthoquinone menadione and *p*-benzoquinone to substitute for sideretin in RoxSR-dependent interactive Fe(III) reduction (Figures 3C–3E, 4G, and S12E). Moreover, lawsone, a naphthoquinone exuded by *Papaver somniferum* under Fe limitation[34]; menadione; and *p*-benzoquinone are direct substrates of NQO1 homologs.[72,89] The model of microbe-mediated redox shuttling of plant-derived sideretin for Fe(III) reduction parallels electron shuttling through bacterial phenazines in other *Pseudomonas* species to enhance phosphorus bioavailability.[68,69,95–97] Thus, microbial redox cycling for soil nutrient mobilization might engage endogenous and exogenous redox mediators. However, the influence of microbial redox cycling on bacterial physiology during nutrient mobilization in the rhizosphere remains to be determined.

The findings presented in this study demonstrate that host-autonomous and pH-dependent exudation of specific coumarins is fully functional for Fe nutrition only in synergy with the bacterial root microbiota. As the bacterial redox and chelation mechanisms described here have likely evolved before the origin of a land plant flora approximately 470 mya,[47–49,98,99] it is possible that exudation of coumarins by non-graminaceous plants reflects an adaptation for Fe acquisition from diverse soils by co-option of ancient microbial processes. The microbial mechanisms identified in this work are generally essential for interbacterial competition and adaption to varying oxygen availability in soil.[47,60,65,83,84] This suggests that coumarin-mediated targeting of these processes in the root microbiota, whose members are recruited from soil at each plant generation, is evolutionarily stable.

Limitations of the study

Although we report a taxonomically widespread ability of root-derived commensal bacteria to rescue Fe deficiency symptoms, we focus on characterizing the mechanism using a single bacterial isolate. Additional mechanisms likely exist in diverse bacteria, which are not characterized here. The precise molecular processes by which IT466 interacts with coumarins to rescue plant Fe starvation also remain to be explored. Specifically, the redox-shuttle mechanism that we propose for sideretin and the Fe shuttle that we propose for bacteria-derived siderophores and fraxetin will need to be experimentally validated in the future. Further, since the mutant screen was performed with menadione rather than sideretin, we would not have identified bacterial mutants that specifically disrupt the bacterial interaction with sideretin but not related quinones. Finally, our study does not address the effect of coumarin interactions on the bacterial Fe status.

RESOURCE AVAILABILITY

Lead contact

Further information and requests for resources and reagents should be addressed to the lead contact, Paul Schulze-Lefert (schlef@mpipz.mpg.de).

Materials availability

This study established a novel *A. thaliana* root-derived bacterial culture collection (At_{IS}-RSPHERE). All other bacterial strains from *At*-RSPHERE[50] and *Arabidopsis* lines used in this study were previously described and are publicly available. Bacterial root isolates and mutants generated in this study will be made available on request to the lead contact.

Data and code availability

Raw sequencing data and assemblies of the bacterial genomes from At_{IS}-RSPHERE and the RNA-seq dataset have been deposited in the European Nucleotide Archive (ENA) under the accession number ENA: PRJEB90850 and will be publicly available upon publication. Datasets and scripts necessary to reproduce analyses and generate figures will be publicly available upon publication at Mendeley Data under the doi: https://doi.org/10.17632/nk4bptx9ft.1, and on GitHub in the repository: https://github.com/charlescopeland/Malisic_Copeland_et_al.git.

ACKNOWLEDGMENTS

This research was funded by the Deutsche Forschungsgemeinschaft (DFG,German Research Foundation) under Germany's Excellence Strategy-EXC 2048-Project IDs: 390686111 and SCHU 799/8-1 (within the priority program SPP 2125 DECRyPT), and the Max Planck Society to P.S.-L. P.S.-L. additionally acknowledges access to the PAM fluorimeter provided by the central facility of the DFG-funded SFB 1403. Additional funding for the establishment of the At_{IS}-RSPHERE culture collection came from the Japan Society for the Promotion of Science (JSPS) KAKENHI (20K05955 and 24K01892), Sumitomo Electric Group CSR Foundation Grant, and Noda Institute for Scientific Research Grant to M.H.

We thank Haruhiko Inoue for support in establishing the At_{IS}-RSPHERE bacterial culture collection and the Max Planck- Genome Centre Cologne for genome sequencing. We thank Dieter Becker, Lucia Schmitz, Shawn Kraemer, Annett Bieber, Maike Grusch, and Sabine Ambrosius for technical support; Mareike J. Kavka and Klaus J. Dehmer for providing IPK soil 1; and Adamo Domenico Rombolà and his group for providing and harvesting the Italian Soil. We also thank Paul Kajdewicz and Lysandros Anastasopoulos for sharing air-tight chambers for bacterial growth under different oxygen concentrations. We appreciate Nicolaus von Wirén's support in coordinating sideretin production

with Orgentis Chemicals GmbH and thank him and Jane E. Parker for helpful discussions. Figures that were created in BioRender: Malisic, M. (2026) (https://BioRender.com/3ge3dg6) and Malisic, M. (2026) (https://BioRender.com/2tennxu).

AUTHOR CONTRIBUTIONS

M.M. and P.S.-L. conceived this study. M.M., C.C., and P.S.-L. designed the experiments. M.M., C.C., A.A., and L.V.D. performed experiments. M.M., C.C., and A.A. analyzed the data. M.M., C.C., and P.S.-L. interpreted the data. M.H. and C.J.H. established the At_{IS}-RSPHERE culture collection. P.Z. curated the At_{IS}-RSPHERE genomes, T.L. performed taxonomic classification, and C.C. inferred phylogenetic relationships for both At_{CAS}- and At_{IS}-RSPHERE. T.L. and N.K. provided bioinformatic support. Y.A.T.M. developed the liquid chromatography-high-resolution mass spectrometry (LC-HRMS) method for coumarin quantification and conducted the analyses. S.K. and S.M. advised and supervised inductively coupled plasma mass spectrometry (ICP-MS) analyses. R.G.-O. advised and supervised computational work on the culture collections and curation of the At_{IS}-RSPHERE culture collection. R.F.H.G. advised and supervised coumarin exudate measurements, analysis, and interpretation of the results; provided scientific advice and rigorous feedback on the manuscript at an early stage; and shared the seeds of *fro2 coumarin pathway* double mutants prior to their publication. P.S.-L. supervised this project. M.M., C.C., and P.S.-L. wrote the manuscript. All co-authors provided feedback on the manuscript.

DECLARATION OF INTERESTS

The authors declare no competing interests.

STAR★METHODS

Detailed methods are provided in the online version of this paper and include the following:

- KEY RESOURCES TABLE
- EXPERIMENTAL MODEL AND STUDY PARTICIPANT DETAILS
  - Soils
  - Bacterial strains and cultivation conditions
  - Plant material and cultivation conditions
- METHOD DETAILS
  - The isolation of bacterial root commensals from *A. thaliana* Col-0 wild type grown in Italian soil and library preparation for whole-genome sequencing
  - Genome assembly and phylogenetic analysis of At_{CAS}- and At_{IS}-RSPHERE culture collection strains
  - Medium preparation for the gnotobiotic plant growth system for Fe limitation
  - Seed sterilization
  - Mono-association screen of At_{CAS}- and At_{IS}-RSPHERE commensals for alleviation of *A. thaliana* Fe deficiency symptoms
  - Photosynthetic efficiency measurements
  - Calculation of rescue activity per strain from the mono-association screen
  - Agar-based gnotobiotic plant growth system for Fe limitation and plant-commensal co-cultivation: Square plate assay
  - SynCom reconstitution
  - Soil experiments
  - Chlorophyll extraction and measurement
  - Mineral composition analysis via ICP-MS
  - Quantification of bacterial abundance by live colony counts
  - *Ex planta* Fe(III) reduction assay using bacterial cells
  - *Ex planta* Fe mobilization assay using bacterial culture supernatants
  - *Ex planta* PVD fluorescence measurements and siderophore activity from Fe-limited bacterial culture supernatants
  - Establishment of an IT466 mini-Tn5 insertion mutant library
  - Forward genetic screen for IT466 mTn5 insertion mutants with diminished menadione-mediated Fe(III) reduction
  - Identification of mini-Tn5 insertion sites
  - Targeted mutagenesis in IT466
  - *In vitro* bacterial growth kinetics
  - Bacterial growth at different oxygen concentrations
  - RNA sequencing for bacterial transcriptomics
  - Root exudate collection
  - Mass spectrometry measurements for coumarin quantification
- QUANTIFICATION AND STATISTICAL ANALYSIS

SUPPLEMENTAL INFORMATION

Supplemental information can be found online at https://doi.org/10.1016/j.cell.2026.09.030.

Received: March 31, 2026
Revised: July 30, 2026
Accepted: September 16, 2026

REFERENCES

1. Lundberg, D.S., Lebeis, S.L., Paredes, S.H., Yourstone, S., Gehring, J., Malfatti, S., Tremblay, J., Engelbrektson, A., Kunin, V., Del Rio, T.G. del, et al. (2012). Defining the core *Arabidopsis thaliana* root microbiome. Nature *488*, 86–90. https://doi.org/10.1038/nature11237.
2. Bulgarelli, D., Schlaeppi, K., Spaepen, S., Ver Loren van Themaat, E.V.L., and Schulze-Lefert, P. (2013). Structure and Functions of the Bacterial Microbiota of Plants. Annu. Rev. Plant Biol. *64*, 807–838. https://doi.org/10.1146/annurev-arplant-050312-120106.
3. Hassani, M.A., Durán, P., and Hacquard, S. (2018). Microbial interactions within the plant holobiont. Microbiome *6*, 58. https://doi.org/10.1186/s40168-018-0445-0.
4. Bulgarelli, D., Rott, M., Schlaeppi, K., Ver Loren van Themaat, E., Ahmadinejad, N., Assenza, F., Rauf, P., Huettel, B., Reinhardt, R., Schmelzer, E., et al. (2012). Revealing structure and assembly cues for *Arabidopsis* root-inhabiting bacterial microbiota. Nature *488*, 91–95. https://doi.org/10.1038/nature11336.
5. Durán, P. (2024). The core microbiota across the green lineage. Curr. Opin. Plant Biol. *77*, 102487. https://doi.org/10.1016/j.pbi.2023.102487.
6. Thiergart, T., Durán, P., Ellis, T., Vannier, N., Garrido-Oter, R., Kemen, E., Roux, F., Alonso-Blanco, C., Ågren, J., Schulze-Lefert, P., et al. (2019). Root microbiota assembly and adaptive differentiation among European Arabidopsis populations. Nat. Ecol. Evol. *4*, 122–131. https://doi.org/10.1038/s41559-019-1063-3.
7. Durán, P., Thiergart, T., Garrido-Oter, R., Agler, M., Kemen, E., Schulze-Lefert, P., and Hacquard, S. (2018). Microbial Interkingdom Interactions in Roots Promote Arabidopsis Survival. Cell *175*, 973–983.e14. https://doi.org/10.1016/j.cell.2018.10.020.
8. Trivedi, P., Leach, J.E., Tringe, S.G., Sa, T., and Singh, B.K. (2020). Plant–microbiome interactions: from community assembly to plant health. Nat. Rev. Microbiol. *18*, 607–621. https://doi.org/10.1038/s41579-020-0412-1.
9. Harbort, C.J., Hashimoto, M., Inoue, H., Niu, Y., Guan, R., Rombolà, A.D., Kopriva, S., Voges, M.J.E.E.E., Sattely, E.S., Garrido-Oter, R., et al. (2020). Root-Secreted Coumarins and the Microbiota Interact to Improve Iron Nutrition in Arabidopsis. Cell Host Microbe *28*, 825–837.e6. https://doi.org/10.1016/j.chom.2020.09.006.
10. Goossens, P., Spooren, J., Baremans, K.C.M., Andel, A., Lapin, D., Echobardo, N., Pieterse, C.M.J., Van den Ackerveken, G., and Berendsen, R.L. (2023). Obligate biotroph downy mildew consistently induces near-identical protective microbiomes in Arabidopsis thaliana. Nat. Microbiol. *8*, 2349–2364. https://doi.org/10.1038/s41564-023-01502-y.
11. Pieterse, C.M.J., Berendsen, R.L., de Jonge, R., Stringlis, I.A., Van Dijken, A.J.H., Van Pelt, J.A., Van Wees, S.C.M., Yu, K., Zamioudis, C., and Bakker, P.A.H.M. (2021). Pseudomonas simiae WCS417: star track

Please cite this article in press as: Malisic et al., *Arabidopsis* uses distinct coumarins and bacterial pathways for pH-adaptive iron acquisition, Cell (2026), https://doi.org/10.1016/j.cell.2026.09.030

of a model beneficial rhizobacterium. Plant Soil *461*, 245–263. https://doi.org/10.1007/s11104-020-04786-9.

12. Van Dijck, L., Esposto, D., Huelsmann, C., Malisic, M., Piro, A., Giehl, R.F.H., Balcke, G.U., Tissier, A., and Parker, J.E. (2025). Cooperation between a root fungal endophyte and host-derived coumarin scopoletin mediates Arabidopsis iron nutrition. New Phytol. *248*, 857–871. https://doi.org/10.1111/nph.70476.

13. Singh, B.K., Hu, H.-W., Macdonald, C.A., and Xiong, C. (2025). Microbiome-facilitated plant nutrient acquisition. Cell Host Microbe *33*, 869–881. https://doi.org/10.1016/j.chom.2025.05.005.

14. Yu, P., He, X., Baer, M., Beirinckx, S., Tian, T., Moya, Y.A.T., Zhang, X., Deichmann, M., Frey, F.P., Bresgen, V., et al. (2021). Plant flavones enrich rhizosphere Oxalobacteraceae to improve maize performance under nitrogen deprivation. Nat. Plants *7*, 481–499. https://doi.org/10.1038/s41477-021-00897-y.

15. Wu, J., Liu, S., Zhang, H., Chen, S., Si, J., Liu, L., Wang, Y., Tan, S., Du, Y., Jin, Z., et al. (2025). Flavones enrich rhizosphere Pseudomonas to enhance nitrogen utilization and secondary root growth in Populus. Nat. Commun. *16*, 1461. https://doi.org/10.1038/s41467-025-56226-w.

16. Copeland, C., Schulze-Lefert, P., and Ma, K.-W. (2025). Potential and challenges for application of microbiomes in agriculture. Plant Cell *37*, koaf185. https://doi.org/10.1093/plcell/koaf185.

17. Li, J., Liu, H., Wang, J., Macdonald, C.A., Singh, P., Cong, V.T., Klein, M., Delgado-Baquerizo, M., and Singh, B.K. (2025). Drought-induced plant microbiome and metabolic enrichments improve drought resistance. Cell Host Microbe *33*, 882–900.e7. https://doi.org/10.1016/j.chom.2025.05.002.

18. Rodriguez, R.J., Henson, J., Van Volkenburgh, E., Hoy, M., Wright, L., Beckwith, F., Kim, Y.-O., and Redman, R.S. (2008). Stress tolerance in plants via habitat-adapted symbiosis. ISME J. *2*, 404–416. https://doi.org/10.1038/ismej.2007.106.

19. Spooren, J., van Bentum, S., Thomashow, L.S., Pieterse, C.M.J., Weller, D.M., and Berendsen, R.L. (2024). Plant-Driven Assembly of Disease-Suppressive Soil Microbiomes. Annu. Rev. Phytopathol. *62*, 1–30. https://doi.org/10.1146/annurev-phyto-021622-100127.

20. Uribe-Acosta, M., Pascale, A., Zhou, J., Stringlis, I.A., and Pieterse, C.M.J. (2025). Roots: metabolic architects of beneficial microbiome assembly. Plant Physiol. *199*, kiaf349. https://doi.org/10.1093/plphys/kiaf349.

21. Bouwmeester, H., Dong, L., Wippel, K., Hofland, T., and Smilde, A. (2025). The chemical interaction between plants and the rhizosphere microbiome. Trends Plant Sci. *30*, 1002–1019. https://doi.org/10.1016/j.tplants.2025.06.001.

22. Marschner, P. (2012). Marschner's Mineral Nutrition of Higher Plants (Elsevier). https://doi.org/10.1016/C2009-0-63043-9.

23. Lindsay, W.L., and Schwab, A.P. (1982). The chemistry of iron in soils and its availability to plants. J. Plant Nutr. *5*, 821–840. https://doi.org/10.1080/01904168209363012.

24. Lemanceau, P., Bauer, P., Kraemer, S., and Briat, J.-F. (2009). Iron dynamics in the rhizosphere as a case study for analyzing interactions between soils, plants and microbes. Plant Soil *321*, 513–535. https://doi.org/10.1007/s11104-009-0039-5.

25. Tsai, H.H., and Schmidt, W. (2017). Mobilization of Iron by Plant-Borne Coumarins. Trends Plant Sci. *22*, 538–548. https://doi.org/10.1016/j.tplants.2017.03.008.

26. Vélez-Bermúdez, I.C., and Schmidt, W. (2023). Plant strategies to mine iron from alkaline substrates. Plant Soil *483*, 1–25. https://doi.org/10.1007/s11104-022-05746-1.

27. Li, M., Watanabe, S., Gao, F., and Dubos, C. (2023). Iron Nutrition in Plants: Towards a New Paradigm? Plants (Basel) *12*, 384. https://doi.org/10.3390/plants12020384.

28. Robinson, N.J., Procter, C.M., Connolly, E.L., and Guerinot, M.L. (1999). A ferric-chelate reductase for iron uptake from soils. Nature *397*, 694–697. https://doi.org/10.1038/17800.

29. Eide, D., Broderius, M., Fett, J., and Guerinot, M.L. (1996). A novel iron-regulated metal transporter from plants identified by functional expression in yeast. Proc. Natl. Acad. Sci. USA *93*, 5624–5628. https://doi.org/10.1073/pnas.93.11.5624.

30. Paffrath, V., Tandron Moya, Y.A., Weber, G., von Wirén, N., and Giehl, R.F.H. (2024). A major role of coumarin-dependent ferric iron reduction in strategy I-type iron acquisition in Arabidopsis. Plant Cell *36*, 642–664. https://doi.org/10.1093/plcell/koad279.

31. Vert, G., Grotz, N., Dédaldéchamp, F., Gaymard, F., Guerinot, M.L., Briat, J.-F., and Curie, C. (2002). IRT1, an Arabidopsis Transporter Essential for Iron Uptake from the Soil and for Plant Growth. Plant Cell *14*, 1223–1233. https://doi.org/10.1105/tpc.001388.

32. Henriques, R., Jásik, J., Klein, M., Martinoia, E., Feller, U., Schell, J., Pais, M.S., and Koncz, C. (2002). Knock-out of Arabidopsis metal transporter gene IRT1 results in iron deficiency accompanied by cell differentiation defects. Plant Mol. Biol. *50*, 587–597. https://doi.org/10.1023/A:1019942200164.

33. Chai, Y.N., and Schachtman, D.P. (2022). Root exudates impact plant performance under abiotic stress. Trends Plant Sci. *27*, 80–91. https://doi.org/10.1016/j.tplants.2021.08.003.

34. Rajniak, J., Giehl, R.F.H., Chang, E., Murgia, I., von Wirén, N., and Sattely, E.S. (2018). Biosynthesis of redox-active metabolites in response to iron deficiency in plants. Nat. Chem. Biol. *14*, 442–450. https://doi.org/10.1038/s41589-018-0019-2.

35. Baune, M., Kang, K., Schenkeveld, W.D.C., Kraemer, S.M., Hayen, H., and Weber, G. (2020). Importance of oxidation products in coumarin-mediated Fe(hydr)oxide mineral dissolution. BioMetals *33*, 305–321. https://doi.org/10.1007/s10534-020-00248-y.

36. Schmid, N.B., Giehl, R.F.H., Döll, S., Mock, H.-P., Strehmel, N., Scheel, D., Kong, X., Hider, R.C., and von Wirén, N. (2014). Feruloyl-CoA 6′-Hydroxylase1-Dependent Coumarins Mediate Iron Acquisition from Alkaline Substrates in Arabidopsis. Plant Physiol. *164*, 160–172. https://doi.org/10.1104/pp.113.228544.

37. Tsai, H.-H., Rodríguez-Celma, J., Lan, P., Wu, Y.-C., Vélez-Bermúdez, I.C., and Schmidt, W. (2018). Scopoletin 8-Hydroxylase-Mediated Fraxetin Production Is Crucial for Iron Mobilization. Plant Physiol. *177*, 194–207. https://doi.org/10.1104/pp.18.00178.

38. Fourcroy, P., Sisó-Terraza, P., Sudre, D., Savirón, M., Reyt, G., Gaymard, F., Abadía, A., Abadia, J., Álvarez-Fernández, A., and Briat, J.-F. (2014). Involvement of the ABCG37 transporter in secretion of scopoletin and derivatives by Arabidopsis roots in response to iron deficiency. New Phytol. *201*, 155–167. https://doi.org/10.1111/nph.12471.

39. Schmidt, H., Günther, C., Weber, M., Spörlein, C., Loscher, S., Böttcher, C., Schobert, R., and Clemens, S. (2014). Metabolome Analysis of Arabidopsis thaliana Roots Identifies a Key Metabolic Pathway for Iron Acquisition. PLOS One *9*, e102444. https://doi.org/10.1371/journal.pone.0102444.

40. Sisó-Terraza, P., Luis-Villarroya, A., Fourcroy, P., Briat, J.-F., Abadía, A., Gaymard, F., Abadía, J., and Álvarez-Fernández, A. (2016). Accumulation and Secretion of Coumarinolignans and other Coumarins in Arabidopsis thaliana Roots in Response to Iron Deficiency at High pH. Front. Plant Sci. *7*, 1711. https://doi.org/10.3389/fpls.2016.01711.

41. Siwinska, J., Siatkowska, K., Olry, A., Grosjean, J., Hehn, A., Bourgaud, F., Meharg, A.A., Carey, M., Lojkowska, E., and Ihnatowicz, A. (2018). Scopoletin 8-hydroxylase: a novel enzyme involved in coumarin biosynthesis and iron-deficiency responses in Arabidopsis. J. Exp. Bot. *69*, 1735–1748. https://doi.org/10.1093/jxb/ery005.

42. Kai, K., Mizutani, M., Kawamura, N., Yamamoto, R., Tamai, M., Yamaguchi, H., Sakata, K., and Shimizu, B. (2008). Scopoletin is biosynthesized via ortho -hydroxylation of feruloyl CoA by a 2-oxoglutarate-dependent

dioxygenase in Arabidopsis thaliana. Plant J. *55*, 989–999. https://doi.org/10.1111/j.1365-313X.2008.03568.x.

43. Vanholme, R., Sundin, L., Seetso, K.C., Kim, H., Liu, X., Li, J., De Meester, B., Hoengenaert, L., Goeminne, G., Morreel, K., et al. (2019). COSY catalyses trans–cis isomerization and lactonization in the biosynthesis of coumarins. Nat. Plants *5*, 1066–1075. https://doi.org/10.1038/s41477-019-0510-0.

44. Tsai, H.-H., and Schmidt, W. (2020). pH-dependent transcriptional profile changes in iron-deficient Arabidopsis roots. BMC Genomics *21*, 694. https://doi.org/10.1186/s12864-020-07116-6.

45. Gautam, C.K., Tsai, H.-H., and Schmidt, W. (2021). IRONMAN tunes responses to iron deficiency in concert with environmental pH. Plant Physiol. *187*, 1728–1745. https://doi.org/10.1093/plphys/kiab329.

46. Gu, S., Wang, N., Zheng, Y., Wang, T., Shen, Q., Zhang, F., Kümmerli, R., Wei, Z., and Zuo, Y. (2025). Integrating microbial siderophores into concepts of plant iron nutrition. Nat. Plants *12*, 26–36. https://doi.org/10.1038/s41477-025-02171-x.

47. Green, J., and Paget, M.S. (2004). Bacterial redox sensors. Nat. Rev. Microbiol. *2*, 954–966. https://doi.org/10.1038/nrmicro1022.

48. Elsen, S., Swem, L.R., Swem, D.L., and Bauer, C.E. (2004). RegB/RegA, a Highly Conserved Redox-Responding Global Two-Component Regulatory System. Microbiol. Mol. Biol. Rev. *68*, 263–279. https://doi.org/10.1128/MMBR.68.2.263-279.2004.

49. Wu, J., and Bauer, C.E. (2008). RegB/RegA, a global redox-responding two-component system. Adv. Exp. Med. Biol. *631*, 131–148. https://doi.org/10.1007/978-0-387-78885-2_9.

50. Bai, Y., Müller, D.B., Srinivas, G., Garrido-Oter, R., Potthoff, E., Rott, M., Dombrowski, N., Münch, P.C., Spaepen, S., Remus-Emsermann, M., et al. (2015). Functional overlap of the Arabidopsis leaf and root microbiota. Nature *528*, 364–369. https://doi.org/10.1038/nature16192.

51. Harbort, C.J., Hashimoto, M., Inoue, H., and Schulze-Lefert, P. (2020). A gnotobiotic growth assay for Arabidopsis root microbiota reconstitution under iron limitation. Star Protoc. *1*, 100226. https://doi.org/10.1016/j.xpro.2020.100226.

52. Nam, H.-I., Shahzad, Z., Dorone, Y., Clowez, S., Zhao, K., Bouain, N., Lay-Pruitt, K.S., Cho, H., Rhee, S.Y., and Rouached, H. (2021). Interdependent iron and phosphorus availability controls photosynthesis through retrograde signaling. Nat. Commun. *12*, 7211. https://doi.org/10.1038/s41467-021-27548-2.

53. Zhao, Q., Liu, F., Xu, J., and Zhang, P. (2026). Identification of miRNAs Responsive to a Defined Period of Iron Deficiency and Resupply in Arabidopsis thaliana. Plants (Basel) *15*, 227. https://doi.org/10.3390/plants15020227.

54. Zhou, C., Guo, J., Zhu, L., Xiao, X., Xie, Y., Zhu, J., Ma, Z., and Wang, J. (2016). Paenibacillus polymyxa BFKC01 enhances plant iron absorption via improved root systems and activated iron acquisition mechanisms. Plant Physiol. Biochem. *105*, 162–173. https://doi.org/10.1016/j.plaphy.2016.04.025.

55. Belkhodja, R., Morales, F., Sanz, M., Abadía, A., and Abadía, J. (1998). Iron deficiency in peach trees: effects on leaf chlorophyll and nutrient concentrations in flowers and leaves. Plant Soil *203*, 257–268. https://doi.org/10.1023/A:1004373202458.

56. Wang, N., Wang, T., Chen, Y., Wang, M., Lu, Q., Wang, K., Dou, Z., Chi, Z., Qiu, W., Dai, J., et al. (2024). Microbiome convergence enables siderophore-secreting-rhizobacteria to improve iron nutrition and yield of peanut intercropped with maize. Nat. Commun. *15*, 839. https://doi.org/10.1038/s41467-024-45207-0.

57. Tan, T., Xu, Z., Tao, L., Sun, X., Xie, J., Miao, Y., Zhang, N., Xun, W., Beauregard, P.B., Kovács, Á.T., et al. (2025). Siderophore-mediated iron enrichment in the biofilm matrix enhances plant iron nutrition. Cell Rep. *44*, 116481. https://doi.org/10.1016/j.celrep.2025.116481.

58. Schalk, I.J. (2025). Bacterial siderophores: diversity, uptake pathways and applications. Nat. Rev. Microbiol. *23*, 24–40. https://doi.org/10.1038/s41579-024-01090-6.

59. Wei, Z., Gu, S., Vollenweider, V., Zuo, Y., Li, Z., and Kümmerli, R. (2025). Microbial siderophores for One Health. Trends Microbiol. *33*, 1277–1285. https://doi.org/10.1016/j.tim.2025.05.002.

60. Kramer, J., Özkaya, Ö., and Kümmerli, R. (2020). Bacterial siderophores in community and host interactions. Nat. Rev. Microbiol. *18*, 152–163. https://doi.org/10.1038/s41579-019-0284-4.

61. Vansuyt, G., Robin, A., Briat, J.-F., Curie, C., and Lemanceau, P. (2007). Iron acquisition from Fe-pyoverdine by Arabidopsis thaliana. Mol. Plant Microbe Interact. *20*, 441–447. https://doi.org/10.1094/MPMI-20-4-0441.

62. Shirley, M., Avoscan, L., Bernaud, E., Vansuyt, G., and Lemanceau, P. (2011). Comparison of iron acquisition from Fe–pyoverdine by strategy I and strategy II plants. Botany *89*, 731–735. https://doi.org/10.1139/b11-054.

63. Nagata, T., Oobo, T., and Aozasa, O. (2013). Efficacy of a bacterial siderophore, pyoverdine, to supply iron to Solanum lycopersicum plants. J. Biosci. Bioeng. *115*, 686–690. https://doi.org/10.1016/j.jbiosc.2012.12.018.

64. Schalk, I.J., and Guillon, L. (2013). Pyoverdine biosynthesis and secretion in Pseudomonas aeruginosa: implications for metal homeostasis. Environ. Microbiol. *15*, 1661–1673. https://doi.org/10.1111/1462-2920.12013.

65. Kawakami, T., Kuroki, M., Ishii, M., Igarashi, Y., and Arai, H. (2010). Differential expression of multiple terminal oxidases for aerobic respiration in Pseudomonas aeruginosa. Environ. Microbiol. *12*, 1399–1412. https://doi.org/10.1111/j.1462-2920.2009.02109.x.

66. Bueno, E., Mesa, S., Bedmar, E.J., Richardson, D.J., and Delgado, M.J. (2012). Bacterial adaptation of respiration from oxic to microoxic and anoxic conditions: redox control. Antioxid. Redox Signal. *16*, 819–852. https://doi.org/10.1089/ars.2011.4051.

67. Emmerich, R., Hennecke, H., and Fischer, H.M. (2000). Evidence for a functional similarity between the two-component regulatory systems RegSR, ActSR, and RegBA (PrrBA) in α-Proteobacteria. Arch. Microbiol. *174*, 307–313. https://doi.org/10.1007/s002030000207.

68. Sporer, A.J., Beierschmitt, C., Bendebury, A., Zink, K.E., Price-Whelan, A., Buzzeo, M.C., Sanchez, L.M., and Dietrich, L.E.P. (2018). Pseudomonas aeruginosa PumA acts on an endogenous phenazine to promote self-resistance. Microbiology (Reading) *164*, 790–800. https://doi.org/10.1099/mic.0.000657.

69. Sakhtah, H., Koyama, L., Zhang, Y., Morales, D.K., Fields, B.L., Price-Whelan, A., Hogan, D.A., Shepard, K., and Dietrich, L.E.P. (2016). The Pseudomonas aeruginosa efflux pump MexGHI-OpmD transports a natural phenazine that controls gene expression and biofilm development. Proc. Natl. Acad. Sci. USA *113*, E3538–E3547. https://doi.org/10.1073/pnas.1600424113.

70. Luscher, A., Gasser, V., Bumann, D., Mislin, G.L.A., Schalk, I.J., and Köhler, T. (2022). Plant-Derived Catechols Are Substrates of TonB-Dependent Transporters and Sensitize Pseudomonas aeruginosa to Siderophore-Drug Conjugates. mBio *13*, e0149822. https://doi.org/10.1128/mbio.01498-22.

71. Fujita, M., Mori, K., Hara, H., Hishiyama, S., Kamimura, N., and Masai, E. (2019). A TonB-dependent receptor constitutes the outer membrane transport system for a lignin-derived aromatic compound. Commun. Biol. *2*, 432. https://doi.org/10.1038/s42003-019-0676-z.

72. Ryan, A., Kaplan, E., Nebel, J.-C., Polycarpou, E., Crescente, V., Lowe, E., Preston, G.M., and Sim, E. (2014). Identification of NAD(P)H Quinone Oxidoreductase Activity in Azoreductases from P. aeruginosa: Azoreductases and NAD(P)H Quinone Oxidoreductases Belong to the Same FMN-Dependent Superfamily of Enzymes. PLOS One *9*, e98551. https://doi.org/10.1371/journal.pone.0098551.

73. Kishko, I., Harish, B., Zayats, V., Reha, D., Tenner, B., Beri, D., Gustavsson, T., Ettrich, R., and Carey, J. (2012). Biphasic Kinetic Behavior of E. coli WrbA, an FMN-Dependent NAD(P)H:Quinone Oxidoreductase. PLOS One *7*, e43902. https://doi.org/10.1371/journal.pone.0043902.

74. Sawers, R.G. (1991). Identification and molecular characterization of a transcriptional regulator from Pseudomonas aeruginosa PAO1 exhibiting structural and functional similarity to the FNR protein of Escherichia coli. Mol. Microbiol. *5*, 1469–1481. https://doi.org/10.1111/j.1365-2958.1991.tb00793.x.

75. Arai, H. (2011). Regulation and Function of Versatile Aerobic and Anaerobic Respiratory Metabolism in Pseudomonas aeruginosa. Front. Microbiol. *2*, 103. https://doi.org/10.3389/fmicb.2011.00103.

76. Arai, H., Kawakami, T., Osamura, T., Hirai, T., Sakai, Y., and Ishii, M. (2014). Enzymatic Characterization and In Vivo Function of Five Terminal Oxidases in Pseudomonas aeruginosa. J. Bacteriol. *196*, 4206–4215. https://doi.org/10.1128/JB.02176-14.

77. Sorescu, J.M., González-Montalvo, M.A., Patel, N., Baltes, G., Avula, S.R., Tuz, K., and Juárez, O.X. (2026). Essential role of cytochrome bc1 in Pseudomonas aeruginosa cell physiology and virulence. Front. Cell. Infect. Microbiol. *16*, 1763669. https://doi.org/10.3389/fcimb.2026.1763669.

78. Comolli, J.C., and Donohue, T.J. (2004). Differences in two Pseudomonas aeruginosa cbb 3 cytochrome oxidases. Mol. Microbiol. *51*, 1193–1203. https://doi.org/10.1046/j.1365-2958.2003.03904.x.

79. Rizaludin, M.S., Stopnisek, N., Raaijmakers, J.M., and Garbeva, P. (2021). The Chemistry of Stress: Understanding the 'Cry for Help' of Plant Roots. Metabolites *11*, 357. https://doi.org/10.3390/metabo11060357.

80. Rolfe, S.A., Griffiths, J., and Ton, J. (2019). Crying out for help with root exudates: adaptive mechanisms by which stressed plants assemble health-promoting soil microbiomes. Curr. Opin. Microbiol. *49*, 73–82. https://doi.org/10.1016/j.mib.2019.10.003.

81. Tharp, C.L., Custer, G.F., Castrillo, G., and Dini-Andreote, F. (2026). Revisiting the cry-for-help hypothesis in plant–microbe interactions. Trends Plant Sci. *31*, 14–16. https://doi.org/10.1016/j.tplants.2025.07.015.

82. Timofeeva, A.M., Galyamova, M.R., and Sedykh, S.E. (2022). Bacterial Siderophores: Classification, Biosynthesis, Perspectives of Use in Agriculture. Plants (Basel) *11*, 3065. https://doi.org/10.3390/plants11223065.

83. Gu, S., Wei, Z., Shao, Z., Friman, V.-P., Cao, K., Yang, T., Kramer, J., Wang, X., Li, M., Mei, X., et al. (2020). Competition for iron drives phytopathogen control by natural rhizosphere microbiomes. Nat. Microbiol. *5*, 1002–1010. https://doi.org/10.1038/s41564-020-0719-8.

84. Getzke, F., Hassani, M.A., Crüsemann, M., Malisic, M., Zhang, P., Ishigaki, Y., Böhringer, N., Jiménez Fernández, A., Wang, L., Ordon, J., et al. (2023). Cofunctioning of bacterial exometabolites drives root microbiota establishment. Proc. Natl. Acad. Sci. USA *120*, e2221508120. https://doi.org/10.1073/pnas.2221508120.

85. Stringlis, I.A., Yu, K., Feussner, K., de Jonge, R., Van Bentum, S., Van Verk, M.C., Berendsen, R.L., Bakker, P.A.H.M., Feussner, I., and Pieterse, C.M.J. (2018). MYB72-dependent coumarin exudation shapes root microbiome assembly to promote plant health. Proc. Natl. Acad. Sci. USA *115*, E5213–E5222. https://doi.org/10.1073/pnas.1722335115.

86. Mortier, V., Holsters, M., and Goormachtig, S. (2012). Never too many? How legumes control nodule numbers. Plant Cell Environ. *35*, 245–258. https://doi.org/10.1111/j.1365-3040.2011.02406.x.

87. Jones, K.M., Kobayashi, H., Davies, B.W., Taga, M.E., and Walker, G.C. (2007). How rhizobial symbionts invade plants: the Sinorhizobium–Medicago model. Nat. Rev. Microbiol. *5*, 619–633. https://doi.org/10.1038/nrmicro1705.

88. Leventhal, G.E., Ackermann, M., and Schiessl, K.T. (2019). Why microbes secrete molecules to modify their environment: the case of iron-chelating siderophores. J. R. Soc. Interface *16*, 20180674. https://doi.org/10.1098/rsif.2018.0674.

89. Green, L.K., La Flamme, A.C., and Ackerley, D.F. (2014). Pseudomonas aeruginosa MdaB and WrbA are water-soluble two-electron quinone oxidoreductases with the potential to defend against oxidative stress. J. Microbiol. *52*, 771–777. https://doi.org/10.1007/s12275-014-4208-8.

90. Patridge, E.V., and Ferry, J.G. (2006). WrbA from Escherichia coli and Archaeoglobus fulgidus Is an NAD(P)H:Quinone Oxidoreductase. J. Bacteriol. *188*, 3498–3506. https://doi.org/10.1128/JB.188.10.3498-3506.2006.

91. Dietrich, L.E.P., Teal, T.K., Price-Whelan, A., and Newman, D.K. (2008). Redox-Active Antibiotics Control Gene Expression and Community Behavior in Divergent Bacteria. Science *321*, 1203–1206. https://doi.org/10.1126/science.1160619.

92. Durchschein, K., Hall, M., and Faber, K. (2013). Unusual reactions mediated by FMN-dependent ene- and nitro-reductases. Green Chem. *15*, 1764. https://doi.org/10.1039/c3gc40588e.

93. Spiegelhauer, O., Mende, S., Dickert, F., Knauer, S.H., Ullmann, G.M., and Dobbek, H. (2010). Cysteine as a Modulator Residue in the Active Site of Xenobiotic Reductase A: a Structural, Thermodynamic and Kinetic Study. J. Mol. Biol. *398*, 66–82. https://doi.org/10.1016/j.jmb.2010.02.044.

94. Vaz, A.D.N., Chakraborty, S., and Massey, V. (1995). Old yellow enzyme: aromatization of cyclic enones and the mechanism of a novel dismutation reaction. Biochemistry *34*, 4246–4256. https://doi.org/10.1021/bi00013a014.

95. Giacalone, D., Schutt, E., and McRose, D.L. (2025). The phospho-ferrozine assay: a tool to study bacterial redox-active metabolites produced at the plant root. Appl. Environ. Microbiol. *91*, e0219424. https://doi.org/10.1128/aem.02194-24.

96. McRose, D.L., Li, J., and Newman, D.K. (2023). The chemical ecology of coumarins and phenazines affects iron acquisition by pseudomonads. Proc. Natl. Acad. Sci. USA *120*, e2217951120. https://doi.org/10.1073/pnas.2217951120.

97. Ciemniecki, J.A., and Newman, D.K. (2023). NADH dehydrogenases are the predominant phenazine reductases in the electron transport chain of Pseudomonas aeruginosa. Mol. Microbiol. *119*, 560–573. https://doi.org/10.1111/mmi.15049.

98. Soares, R., Trindade, I.B., and Louro, R.O. (2026). Iron Binding before Iron Limitation: Siderophore synthesis arose well before iron became a limiting element. ISME Commun. *6*, ycag025. https://doi.org/10.1093/ismeco/ycag025.

99. Bowman, J.L. (2022). The origin of a land flora. Nat. Plants *8*, 1352–1369. https://doi.org/10.1038/s41477-022-01283-y.

100. Merrell, D.S., Hava, D.L., and Camilli, A. (2002). Identification of novel factors involved in colonization and acid tolerance of Vibrio cholerae. Mol. Microbiol. *43*, 1471–1491. https://doi.org/10.1046/j.1365-2958.2002.02857.x.

101. Varotto, C., Maiwald, D., Pesaresi, P., Jahns, P., Salamini, F., and Leister, D. (2002). The metal ion transporter IRT1 is necessary for iron homeostasis and efficient photosynthesis in Arabidopsis thaliana. Plant J. *31*, 589–599. https://doi.org/10.1046/j.1365-313X.2002.01381.x.

102. Bankevich, A., Nurk, S., Antipov, D., Gurevich, A.A., Dvorkin, M., Kulikov, A.S., Lesin, V.M., Nikolenko, S.I., Pham, S., Prjibelski, A.D., et al. (2012). SPAdes: A New Genome Assembly Algorithm and Its Applications to Single-Cell Sequencing. J. Comput. Biol. *19*, 455–477. https://doi.org/10.1089/cmb.2012.0021.

103. Parks, D.H., Imelfort, M., Skennerton, C.T., Hugenholtz, P., and Tyson, G.W. (2015). CheckM: assessing the quality of microbial genomes recovered from isolates, single cells, and metagenomes. Genome Res. *25*, 1043–1055. https://doi.org/10.1101/gr.186072.114.

104. Kang, D.D., Li, F., Kirton, E., Thomas, A., Egan, R., An, H., and Wang, Z. (2019). MetaBAT 2: An adaptive binning algorithm for robust and efficient genome reconstruction from metagenome assemblies. PeerJ *7*, e7359. https://doi.org/10.7717/peerj.7359.

105. Olm, M.R., Brown, C.T., Brooks, B., and Banfield, J.F. (2017). dRep: a tool for fast and accurate genomic comparisons that enables improved genome recovery from metagenomes through de-replication. ISME J. *11*, 2864–2868. https://doi.org/10.1038/ismej.2017.126.

106. Hunt, M., Silva, N.D., Otto, T.D., Parkhill, J., Keane, J.A., and Harris, S.R. (2015). Circlator: automated circularization of genome assemblies using long sequencing reads. Genome Biol. *16*, 294. https://doi.org/10.1186/s13059-015-0849-0.

107. Seemann, T. (2014). Prokka: rapid prokaryotic genome annotation. Bioinformatics *30*, 2068–2069. https://doi.org/10.1093/bioinformatics/btu153.

108. Wu, M., and Scott, A.J. (2012). Phylogenomic analysis of bacterial and archaeal sequences with AMPHORA2. Bioinformatics *28*, 1033–1034. https://doi.org/10.1093/bioinformatics/bts079.

109. Price, M.N., Dehal, P.S., and Arkin, A.P. (2009). FastTree: Computing Large Minimum Evolution Trees with Profiles instead of a Distance Matrix. Mol. Biol. Evol. *26*, 1641–1650. https://doi.org/10.1093/molbev/msp077.

110. Chen, S. (2023). Ultrafast one-pass FASTQ data preprocessing, quality control, and deduplication using fastp. Imeta *2*, e107. https://doi.org/10.1002/imt2.107.

111. Kim, D., Paggi, J.M., Park, C., Bennett, C., and Salzberg, S.L. (2019). Graph-based genome alignment and genotyping with HISAT2 and HISAT-genotype. Nat. Biotechnol. *37*, 907–915. https://doi.org/10.1038/s41587-019-0201-4.

112. Liao, Y., Smyth, G.K., and Shi, W. (2014). featureCounts: an efficient general purpose program for assigning sequence reads to genomic features. Bioinformatics *30*, 923–930. https://doi.org/10.1093/bioinformatics/btt656.

113. Love, M.I., Huber, W., and Anders, S. (2014). Moderated estimation of fold change and dispersion for RNA-seq data with DESeq2. Genome Biol. *15*, 550. https://doi.org/10.1186/s13059-014-0550-8.

114. Virtanen, P., Gommers, R., Oliphant, T.E., Haberland, M., Reddy, T., Cournapeau, D., Burovski, E., Peterson, P., Weckesser, W., Bright, J., et al. (2020). SciPy 1.0: fundamental algorithms for scientific computing in Python. Nat. Methods *17*, 261–272. https://doi.org/10.1038/s41592-019-0686-2.

115. Jones, P., Binns, D., Chang, H.-Y., Fraser, M., Li, W., McAnulla, C., McWilliam, H., Maslen, J., Mitchell, A., Nuka, G., et al. (2014). InterProScan 5: genome-scale protein function classification. Bioinformatics *30*, 1236–1240. https://doi.org/10.1093/bioinformatics/btu031.

116. Alexa, A., Rahnenführer, J., and Lengauer, T. (2006). Improved scoring of functional groups from gene expression data by decorrelating GO graph structure. Bioinformatics *22*, 1600–1607. https://doi.org/10.1093/bioinformatics/btl140.

117. Kvitko, B.H., and Collmer, A. (2011). Construction of Pseudomonas syringae pv. tomato DC3000 Mutant and Polymutant Strains. Methods Mol. Biol. *712*, 109–128. https://doi.org/10.1007/978-1-61737-998-7_10.

118. Yi, Y., and Guerinot, M.L. (1996). Genetic evidence that induction of root Fe(III) chelate reductase activity is necessary for iron uptake under iron deficiency. Plant J. *10*, 835–844. https://doi.org/10.1046/j.1365-313X.1996.10050835.x.

119. Wippel, K., Tao, K., Niu, Y., Zgadzaj, R., Kiel, N., Guan, R., Dahms, E., Zhang, P., Jensen, D.B., Logemann, E., et al. (2021). Host preference and invasiveness of commensal bacteria in the Lotus and Arabidopsis root microbiota. Nat. Microbiol. *6*, 1150–1162. https://doi.org/10.1038/s41564-021-00941-9.

120. Durán, P., Flores-Uribe, J., Wippel, K., Zhang, P., Guan, R., Melkonian, B., Melkonian, M., and Garrido-Oter, R. (2022). Shared features and reciprocal complementation of the Chlamydomonas and Arabidopsis microbiota. Nat. Commun. *13*, 406. https://doi.org/10.1038/s41467-022-28055-8.

121. Kanehisa, M., Goto, S., Kawashima, S., and Nakaya, A. (2002). The KEGG databases at GenomeNet. Nucleic Acids Res. *30*, 42–46. https://doi.org/10.1093/nar/30.1.42.

122. Chaumeil, P.-A., Mussig, A.J., Hugenholtz, P., and Parks, D.H. (2019). GTDB-Tk: a toolkit to classify genomes with the Genome Taxonomy Database. Bioinformatics *36*, 1925–1927. https://doi.org/10.1093/bioinformatics/btz848.

123. Letunic, I., and Bork, P. (2021). Interactive Tree Of Life (iTOL) v5: an online tool for phylogenetic tree display and annotation. Nucleic Acids Res. *49*, W293–W296. https://doi.org/10.1093/nar/gkab301.

124. Abadía, J., Morales, F., and Abadía, A. (1999). Photosystem II efficiency in low chlorophyll, iron-deficient leaves. Plant Soil *215*, 183–192. https://doi.org/10.1023/A:1004451728237.

125. Zhang, H., Sun, Y., Xie, X., Kim, M.-S., Dowd, S.E., and Paré, P.W. (2009). A soil bacterium regulates plant acquisition of iron via deficiency-inducible mechanisms. Plant J. *58*, 568–577. https://doi.org/10.1111/j.1365-313X.2009.03803.x.

126. Gruber, B.D., Giehl, R.F.H., Friedel, S., and von Wirén, N. (2013). Plasticity of the Arabidopsis Root System under Nutrient Deficiencies. Plant Physiol. *163*, 161–179. https://doi.org/10.1104/pp.113.218453.

127. Hiscox, J.D., and Israelstam, G.F. (1979). A method for the extraction of chlorophyll from leaf tissue without maceration. Can. J. Bot. *57*, 1332–1334. https://doi.org/10.1139/b79-163.

128. Almario, J., Jeena, G., Wunder, J., Langen, G., Zuccaro, A., Coupland, G., and Bucher, M. (2017). Root-associated fungal microbiota of nonmycorrhizal Arabis alpina and its contribution to plant phosphorus nutrition. Proc. Natl. Acad. Sci. USA *114*, E9403–E9412. https://doi.org/10.1073/pnas.1710455114.

129. Ma, K.W., Ordon, J., and Schulze-Lefert, P. (2022). Gnotobiotic Plant Systems for Reconstitution and Functional Studies of the Root Microbiota. Curr. Protoc. *2*, e362. https://doi.org/10.1002/cpz1.362.

130. Schwyn, B., and Neilands, J.B. (1987). Universal chemical assay for the detection and determination of siderophores. Anal. Biochem. *160*, 47–56. https://doi.org/10.1016/0003-2697(87)90612-9.

131. Light, S.H., Su, L., Rivera-Lugo, R., Cornejo, J.A., Louie, A., Iavarone, A.T., Ajo-Franklin, C.M., and Portnoy, D.A. (2018). A flavin-based extracellular electron transfer mechanism in diverse Gram-positive bacteria. Nature *562*, 140–144. https://doi.org/10.1038/s41586-018-0498-z.

132. Ordon, J., Logemann, E., Maier, L.-P., Lee, T., Dahms, E., Oosterwijk, A., Flores-Uribe, J., Miyauchi, S., Paoli, L., Stolze, S.C., et al. (2025). Conserved immunomodulation and variation in host association by Xanthomonadales commensals in Arabidopsis root microbiota. Nat. Plants *11*, 612–631. https://doi.org/10.1038/s41477-025-01918-w.

133. Ashburner, M., Ball, C.A., Blake, J.A., Botstein, D., Butler, H., Cherry, J.M., Davis, A.P., Dolinski, K., Dwight, S.S., Eppig, J.T., et al. (2000). Gene Ontology: tool for the unification of biology. The Gene Ontology Consortium. Nat. Genet. *25*, 25–29. https://doi.org/10.1038/75556.

Please cite this article in press as: Malisic et al., *Arabidopsis* uses distinct coumarins and bacterial pathways for pH-adaptive iron acquisition, Cell (2026), https://doi.org/10.1016/j.cell.2026.09.030

CellPress
OPEN ACCESS

STAR★METHODS

KEY RESOURCES TABLE

REAGENT or RESOURCE	SOURCE	IDENTIFIER
Bacterial and virus strains		
At-RSPHERE (here At_{CAS}-RSPHERE), *A. thaliana* root-derived bacterial culture collection, Table S1	Bai et al.[50]	http://www.at-sphere.com/
At_{IS}-RSPHERE, *A. thaliana* root-derived bacterial culture collection, Table S1	This study	N/A
Escherichia coli BW29427	*E. coli* Genetic Resource Center (CGSC)	CGSC #14194
Escherichia coli M10λpir carrying pUTmTn5Km2	Merrel et al.[100]	N/A
Pseudomonas proteolytica IT466 mTn5 library	This study	N/A
Pseudomonas proteolytica IT466 Δ*pvdD*	This study	N/A
Pseudomonas proteolytica IT466 Δ*roxR*	This study	N/A
Pseudomonas proteolytica IT466 Δ*roxS*	This study	N/A
Pseudomonas proteolytica IT466 Δ*roxSR*	This study	N/A
Pseudomonas proteolytica IT466 Δ*anr*	This study	N/A
Pseudomonas proteolytica IT466 Δ*petCBA*	This study	N/A
Pseudomonas proteolytica IT466 Δ*cco-1/-2*	This study	N/A
Pseudomonas proteolytica IT466 *roxR*::mTn5	This study	N/A
Biological samples		
IPKS1, soil	This study	N/A
IPKS1, soil	This study	N/A
CAS, soil	This study	N/A
IS, soil	This study	N/A
Chemicals, peptides, and recombinant proteins		
NaEDTA	Sigma-Aldrich	CAT#E6635
Ascorbic acid	Sigma-Aldrich	CAT#A92902
Scopoletin	Sigma-Aldrich	CAT#S2500
Fraxetin	Sigma-Aldrich	CAT#254916
Esculetin	Sigma-Aldrich	CAT#246573
Sideretin, custom synthesis	Orgentis Chemicals GmbH	N/A
Menadione	Sigma-Aldrich	CAT#M5625
Menadiol	fluorochem	CAT#F542398
p-Benzoquinone	Sigma-Aldrich	CAT#B10358
Hydroquinone	Sigma-Aldrich	CAT#H9003
Palladium	Sigma-Aldrich	CAT#203998
FeNaEDTA	Sigma-Aldrich	CAT#E6760
$FeCl_3$ hexahydrate	ROTH	CAT#P742.1
Ferrozine	Sigma-Aldrich	CAT#160601
Bacto Agar	BD	CAT#214010
Technical Agar	BD	CAT#281230
Bacteriological Agar	BD	CAT#214530; LOT:3004934, 3168361
MES buffer	Duchefa Biochemie	CAT#M1503

(*Continued on next page*)

Continued

REAGENT or RESOURCE	SOURCE	IDENTIFIER
HEPES buffer	ROTH	CAT#6763.1
MS medium including vitamins, for pre-germination	Duchefa Biochemie	CAT#M0222
Custom ½ MS protocol	Harbort et al.[9]	N/A
Fe-limiting culture medium bacteria, siderophore medium	Table S5 in Getzke et al.[84]	N/A
Tryptic Soy Broth	Millipore	CAT#T8907
Critical commercial assays		
ReliaPrep™ RNA Cell Miniprep System	Promega	Z6012
Deposited data		
Raw and processed data, scripts for analysis and figure generation	This study	Mendeley Data: https://doi.org/10.17632/nk4bptx9ft.1.
Bacterial RNA-Seq data	This study	ENA: PRJEB90850
AtIS-RSPHERE culture collection whole genome sequence data	This study	ENA: PRJEB90850
Experimental models: Organisms/strains		
A. thaliana: Col-0 wildtype	NASC	N60000
A. thaliana: *f6'h1-1*	NASC	SALK_132418C
A. thaliana: *s8h-2*	Rajniak et al.[34]	SM_3_23443
A. thaliana: *cyp82C4-2*	NASC	SALK_001585
A. thaliana fro2 (frd1-1)	NASC	N3777
A. thaliana: fro2 f6'h1-1	Paffrath et al.[30]	N/A
A. thaliana: fro2 s8h-1	Paffrath et al.[30]	N/A
A. thaliana: fro2 cyp82C4-1	Paffrath et al.[30]	N/A
A. thaliana: Col-gl1	NASC	N3879
A. thaliana: Col-0xCol-gl1	Paffrath et al.[30]	N/A
A. thaliana: irt1-1	Varotto et al.[101]	N/A
Oligonucleotides		
All primers used are listed in Table S14	N/A	N/A
Software and algorithms		
ImagingWin v2.56	Walz, Germany	N/A
R statistical environment v4.4	https://www.r-project.org/	N/A
Python v3.12	https://www.python.org/	N/A
SPAdes v3.15.2	Bankevich et al.[102]	https://github.com/ablab/spades
CheckM v1.2.2	Parks et al.[103]	https://github.com/ecogenomics/checkm
MetaBAT 2 v2.13	Kang et al.[104]	https://bioconda.github.io/recipes/metabat2/README.html
dRep v3.2.0	Olm et al.[105]	https://github.com/MrOlm/drep
circlator v1.5.5	Hunt et al.[106]	https://github.com/sanger-pathogens/circlator
Prokka v1.14.5	Seemann et al.[107]	https://github.com/tseemann/prokka
AMPHORA2	Wu and Scott[108]	https://github.com/wu-lab-uva/AMPHORA2
FastTree 2.1.11	Price et al.[109]	https://github.com/morgannprice/fasttree
fastp v0.23.4	Chen[110]	https://github.com/opengene/fastp
HISAT2 v2.1.0	Kim et al.[111]	https://github.com/DaehwanKimLab/hisat2
featureCounts v2.0.2	Liao et al.[112]	https://bioconductor.org/packages/release/bioc/html/Rsubread.html

(*Continued on next page*)

Please cite this article in press as: Malisic et al., *Arabidopsis* uses distinct coumarins and bacterial pathways for pH-adaptive iron acquisition, Cell (2026), https://doi.org/10.1016/j.cell.2026.09.030

CellPress
OPEN ACCESS

Continued

REAGENT or RESOURCE	SOURCE	IDENTIFIER
DESeq2 R package v1.46.0	Love et al.[113]	https://bioconductor.org/packages/release/bioc/html/DESeq2.html
SciPy v1.14.0	Virtanen et al.[114]	https://scipy.org/
interproscan v5.76-107.0	Jones et al.[115]	https://www.ebi.ac.uk/interpro/download/InterProScan/
topGO v2.58.0	Alexa et al.[116]	https://bioconductor.org/packages/release/bioc/html/topGO.html
Custom python scripts	This paper	https://github.com/charlescopeland/Malisic_Copeland_et_al
Other		
pK18*mobsacB* cloning vector	Kvitko and Collmer[117]	Genebank accession: FJ437239

EXPERIMENTAL MODEL AND STUDY PARTICIPANT DETAILS

Soils

Italian soil (IS) was retrieved from an organic vineyard in Tebano, Italy (GPS code: 44.292 N, 11.784 E). This vineyard has been maintained since 2007 without irrigation or fertilization. Cologne agricultural soil (CAS) was obtained from a local site (GPS code: 50.958 N, 6.856 E) that has not been exposed to agriculture for >15 years. IPK soil 1 pH 5.7 was retrieved from an experimental field in Groß Lüsewitz, Germany (GPS code: 54.070 N, 12.324 E) and IPK soil 2 pH 7.2 from Gatersleben, Germany (GPS code: 51.829 N, 11.271 E). Both soils have been cultivated without irrigation and minimal nutrient inputs since >10 years. All soils were homogenized, sieved, and stored at 4°C until used for experiments.

Bacterial strains and cultivation conditions

All bacterial strains used were root isolates of *A. thaliana* from the *At*-RSPHERE[50] collection (here: At_{CAS}-RSPHERE) and the At_{IS}-RSPHERE collection, established in this study. A full list of strains with taxonomic classification is provided in Table S1. Strains were stored long-term in 30% glycerol at -80°C and short-term on 50% TSA plates (1.5% Bacto agar, BD) at 4°C. For experiments, bacteria were revived from glycerol stocks on 50% TSA plates (1.5% Bacto agar, BD) at 25°C for 2–5 days. Single colonies were cultivated in 50% TSB at 25°C under agitation at 180 rpm for 1–3 days.

Plant material and cultivation conditions

Columbia-0 wild-type (Col-0; NASC: N60000) and the following homozygous T-DNA insertion lines in the Col-0 background were used in this study: *f6'h1-1* (AT3G13610; SALK_132418C),[36] *s8h-1* (AT3G12900; SM_3_27151),[34] *s8h-2* (AT3G12900; SM_3_23443),[34] *cyp82C4-1* (AT4G31940; SALK_001585),[34] and *irt1* (AT4G19690).[101] Furthermore, *fro2* (*frd1-1*; NASC: N3777)[118] and the Columbia *glabra-1* (Col-*gl1*) background and homozygous *fro2* coumarin biosynthesis pathway double mutants derived from crosses generated previously by Paffrath et al.,[30] *fro2 f6'h1-1*, *fro2 s8h-2*, *fro2 cyp82C4-1*, and the corresponding wild type Col-0xCol-*gl1* were used in this study. Soil experiments were performed in the greenhouse under short-day conditions (8/16 hours day/night cycle). In all other experiments, plants were cultivated in gnotobiotic growth systems in a climate chamber (Panasonic, MLR-352) with 60% humidity at a 10/14 hours day/night cycle with a day temperature of 21°C and night temperature 19°C. Continuous LED light of 80–100 μmol photons s^{-2} m^{-2} was used for illumination. Plants in the climate chamber were grown vertically on square petri plates (12x12 cm) or on 24 well-plates (mono-association screen).

METHOD DETAILS

The isolation of bacterial root commensals from *A. thaliana* Col-0 wild type grown in Italian soil and library preparation for whole-genome sequencing

At_{IS}-RSPHERE was established from two independent isolation events. The procedures of bacterial isolation, DNA extraction and high-throughput strain identification using Roche 454 Genome sequencer GS FLX+ were performed as described previously.[50] *A. thaliana* Col-0 plants were grown in Italian soil 1st batch for seven weeks in the greenhouse. We obtained four independent biological replicates (five individual plants in each replicate) throughout the two isolation events. Roots from another five independent plants were used for culture-independent community profiling based on 16S rRNA amplicon sequencing. Root samples were washed twice using 10 mM $MgCl_2$ with shaking for 20 min. Dried root samples were crushed at 5,600 rpm for 30 seconds, and mixed with 50 mL of 10 mM $MgCl_2$. After 15 min sedimentation in a plastic tube, the supernatant was diluted at 1,200 times using 50% TSB, and cultivated in 96-well plates for three weeks. After close referencing of sequence-indexed rhizobacteria library (approximately 3,700 colony-forming units) sequences with culture-independent community profiling, candidate strains with 97% or higher 16S rRNA gene identity to the

OTUs found in amplicon sequencing data were retrieved from the 96-well glycerol stock, and were purified by three rounds of consecutive streaking. After verifying the identity of the isolated strains, single tube glycerol stocks were prepared for each strain. Bacterial genomic DNA purification was performed as described previously.[50] Sequencing library construction and whole genome sequencing using Illumina Hiseq3000 platform were performed by the Max Planck Genome Center, Cologne, Germany.

Genome assembly and phylogenetic analysis of At_{CAS}- and At_{IS}-RSPHERE culture collection strains

To assemble the bacterial genomes, we used SPAdes (v3.15.2)[102] with raw Illumina paired-end FASTQ files as input. We assessed the completeness and the contamination rate of the assembled genomes using CheckM (v1.2.2).[103] Genomes with more than 90% completeness and less than 10 contamination rate were classified as high-quality. For genomes with high contamination rates, we treated them as metagenomic sequences, as they might be a mixture of genomes. We employed the metagenome binning software MetaBAT 2 (v2.13)[104] for this decontamination process. Genomes were labeled as ITX_Y, where X is the strain identifier and Y is the metagenomic bin identifier. Post-decontamination, we reassessed their quality with CheckM, including only those meeting our criteria for further processing. We removed redundant genomes from the high-quality and decontaminated set using dRep (v3.2.0)[105] with specific parameters: -pa 0.999—SkipSecondary -p 20—ignoreGenomeQuality -ms 5000 -centW 0 -sizeW 1. The whole above-mentioned cleaning process resulted in 140 genomes. Genome assemblies were reoriented using circlator fixstart (v1.5.5),[106] positioning the replication initiator gene *dnaA* at the start of each assembly, using a custom *dnaA* reference database compiled from previously established culture collections.[50,119,120] Functional annotation was performed with Prokka (v1.14.5),[107] using an in-house KEGG ontology database.[121] The resulting GFF3 files were parsed using custom Python scripts. In annotation files from this pipeline (e.g. Table S4 for IT466), *roxR* (KO K15012) and *roxS* (KO K15011) are listed as *regA* and *regB*, respectively, following the naming of the homologs from *Rhodobacter capsulatus*.[48,49] For both culture collections (At_{CAS}- and At_{IS}-RSPHERE) strain taxonomy was annotated using GTDB-Tk v2.7.1 with GTDB reference data release r232.[122] For phylogenetic analysis of At_{CAS}- and At_{IS}-derived commensals was based on 31 bacterial marker genes were aligned using AMPHORA2[108] The tree was created with FastTree[109] and the tree was rooted at the midpoint and visualized with the online tool iTOL v5.[123]

Medium preparation for the gnotobiotic plant growth system for Fe limitation

Plant growth medium was based on half-strength Murashige and Skoog (MS) medium was prepared from self-made stock solutions and supplemented with 1% agar (Difco Agar Bacteriological, BD) as described in Harbort et al.[9,51] and autoclaved. No Fe or pH buffer was added initially. Autoclaved media were then supplemented with Fe and buffer from sterile-filtered stock solutions depending on the desired Fe (bio)availability and pH. For acidic conditions (pH 5.7), MES was added to a final concentration of 5 mM from a 1 M stock solution (stock pH 6.0). For circumneutral pH conditions (pH 7.4), HEPES was added to a final concentration of 10 mM from a 2 M stock solution (stock pH 8.3). Fe was supplied at 50 or 100 μM as $FeCl_3$ (unavFe) or equimolar concentrations of FeNaEDTA (avFe), or at 1 μM FeNaEDTA (insufficient Fe), from filter-sterilized 100 mM stock solutions prepared in 10 mM HCl. The medium was cooled to ~45 °C and used for both square plate (12x12 cm) and 24-well plate screening experiments.

Seed sterilization

Seeds (>250 μm) were surface sterilized with 70% ethanol for 30 min under over-head rotation and subsequently washed twice with 70% ethanol and once with 100% ethanol prior to four times washing with sterile deionized water. Sterilized seeds were stratified for two to three days at 4°C either on agar media plates (for square plate assay experiments) or in sterile deionized water (for 24 well-plate experiments).

Mono-association screen of At_{CAS}- and At_{IS}-RSPHERE commensals for alleviation of *A. thaliana* Fe deficiency symptoms

Individual bacteria from At_{CAS}- and At_{IS}-RSPHERE were precultured for three days, harvested by centrifugation (4,000 x g, 10 min, room temperature), washed once with 10 mM $MgCl_2$, and resuspended in 10 mM $MgCl_2$. Cell density was determined spectrophotometrically (OD_{600}) and adjusted to either OD_{600} = 1 (100-fold stock for final OD_{600} = 0.01 in plant growth medium) or OD_{600} = 0.01 (100-fold stock for final OD_{600} = 0.0001 in plant growth medium). Two surface-sterilized, cold-stratified *A. thaliana* Col-0 wild type seeds were placed in each well of a 24-well plate containing ½ MS medium supplemented with Fe and buffer: 50 μM $FeCl_3$ and 5 mM MES (pH 5.7) for acidic conditions or 100 μM $FeCl_3$ and 10 mM HEPES (pH 7.4) for circumneutral conditions and the bacterial inoculum. Axenic plants ($MgCl_2$ control inoculated) grown with FeEDTA or $FeCl_3$ served as positive and negative rescue controls, respectively. Each strain was inoculated in four biological replicates per inoculum titer per experiment. Plates were cultivated vertically for three weeks under short-day conditions (10 h light / 14 h dark) before assessment of the maximum quantum efficiency of photosystem II (F_v/F_m) as a physiological indicator for Fe deficiency symptoms.[52–54,124,125] The same procedure was applied for mono-association screens using *fro2* plants (100 μM $FeCl_3$, pH 5.7, 5 mM MES). A complete table of all strains, their taxonomy and assigned rescue categories for each plant genotype and pH condition is provided (Table S1).

Additionally, a subset of strains was assessed for their effects on the F_v/F_m parameter under avFe, using 50 μM FeEDTA and 5 mM MES (pH 5.7) for acidic conditions or 100 μM FeEDTA and 10 mM HEPES (pH 7.4) for circumneutral conditions.

Please cite this article in press as: Malisic et al., *Arabidopsis* uses distinct coumarins and bacterial pathways for pH-adaptive iron acquisition, Cell (2026), https://doi.org/10.1016/j.cell.2026.09.030

Photosynthetic efficiency measurements

The maximum quantum efficiency of photosystem II is represented by the F_v/F_m ratio and was measured with the MAXI version IMAGING-PAM fluorometer (WALZ, Germany) using the ImagingWin Software v2.41a (WALZ, Germany). Three-week-old seedlings were dark-adapted for 20 min prior to the measurement. F_0 (minimal fluorescence for the dark-adapted state) was acquired. Afterwards, the maximal level of fluorescence in dark-adapted state (F_M) was measured by applying a saturating light-pulse. The F_v/F_m ($F_v = F_m - F_o$) value was automatically calculated by the ImagingWin software and was extracted for the 24-well format simultaneously for all wells. The F_v/F_m values were then used to calculate rescue activities of each bacterial strain tested.

Calculation of rescue activity per strain from the mono-association screen

The host rescue activity of each strain in % was calculated similarly to Harbort et al.,[9] using the following formula:

$$\%\ Rescue\ activity = \frac{\left(Fv/Fm_{inoculated\ on\ unavFe} - Fv/Fm_{axenic\ on\ unavFe}\right)}{\left(Fv/Fm_{axenic\ on\ avFe} - Fv/Fm_{axenic\ on\ unavFe}\right)} \times 100.$$

Each strain's rescue activity was assessed in four biological replicates per inoculum titer and a strain was defined as rescuing commensal if i) the rescue activity was $\geq$ 50% in at least two out of four biological replicates, ii) in at least one of the two inoculum titers. Rescue properties of each strain are listed in Table S1.

Agar-based gnotobiotic plant growth system for Fe limitation and plant-commensal co-cultivation: Square plate assay

A. thaliana seeds were pre-germinated under sterile conditions on ½ MS medium (2.2 g/L MS with vitamins, Duchefa; 5 g/L sucrose; 0.6 g/L MES; pH 5.7; 1% Bacto agar, BD) and stratified for 2 days at 4°C, followed by 7 days of light exposure. Pre-germinated seedlings of a similar developmental stage were then transferred to agar-based gnotobiotic plates for microbiota reconstitution experiments under differential Fe and pH conditions (5–6 seedlings per plate). For bacterial co-cultivation, *Pseudomonas* IT466 or individual SynCom members (Table S6) were precultured, harvested (4,000 × *g*, 10 min, room temperature), washed in 10 mM $MgCl_2$, and resuspended. Stock OD_{600} was adjusted according to the experiment (OD_{600} = 0.1 for IT466, then diluted to a final OD_{600} = 0.0001 in plates). As a germ-free control, IT466 (OD_{600} = 0.1) was heat-killed (99°C, 60 min) and inoculated at the same titer as live IT466. The SynCom reconstitution procedure for the SynCom experiments is described in the section below. Where indicated in the figures and figure legends, chemical supplements such as coumarins and corresponding controls were added to the medium at 50 or 100 μM, with a 1:1 DMSO:water control as mock treatment. Seedlings and bacteria were co-cultivated vertically in plant cultivation chambers for 2 weeks prior to phenotypic assessment.

As variation in agar mineral nutrients can have confounding effects on plant phenotypes under nutrient limitation[126] and may affect plant phenotypes under Fe-limiting conditions, we recommend that the amount of added Fe should be adjusted to each new agar batch. This is especially relevant to detect differential rescue activities between wild-type and mutant bacteria.

SynCom reconstitution

Each SynCom contained a mixture of strains with contrasting *fro2* rescue activities, as defined by the mono-association screen. For SynCom1 and SynCom2, non-rescuing strains were combined at equal densities to form a non-rescuing SynCom (nrSC), and rescuing strains were combined similarly to form a rescuing SynCom (rSC). The nrSC and rSC were then mixed in equal amounts to generate the final SynCom. SynComs were inoculated into the medium at a total OD_{600} of 0.0002, with the nrSC and rSC each contributing OD_{600} = 0.0001. SynCom3, the only SynCom containing IT466, was prepared by combining all members at equal densities to a final OD_{600} of 0.0002. A complete list of SynCom members is provided in Table S6.

Soil experiments

Surface-sterilized, stratified seeds (5 days) were germinated in 9 × 9 cm square pots filled with CAS (pH 6.5), IS (pH 7.5), IPKS1 (pH 5.7), or IPKS2 (pH 7.2) substrates. Pots were bottom-watered with deionized water every three days. Plants were cultivated for 35 days after germination (dag) in a greenhouse under short-day conditions (8 h light/16 h dark). Pots were randomly distributed within trays and repositioned regularly to minimize edge and positional effects. At 35 dag, 5–6 plants were pooled per sample to determine shoot fresh weight per plant. In addition, shoot samples (each comprising leaves from 5–6 plants per pot) were collected for chlorophyll extraction and quantification.

Chlorophyll extraction and measurement

Shoot chlorophyll was extracted and quantified as previously described.[9,127] In brief, samples were prepared from 5–40 mg shoot tissue of five-six plants from one square plate (one biological replicate per plate) or from the same amount of plants grown in soils (two samples per pot). Chlorophyll was extracted in 1 mL DMSO per 30 mg leaf tissue and samples were incubated at 65°C for 45 min under agitation until leaves became transparent. The absorbance of the chlorophyll extract was measured at 652 nm with a spectrophotometer (NanoDrop One, Thermo Scientific) and the total chlorophyll concentration normalized to shoot fresh weight was calculated as described in Harbort et al.[9,51]

Please cite this article in press as: Malisic et al., *Arabidopsis* uses distinct coumarins and bacterial pathways for pH-adaptive iron acquisition, Cell (2026), https://doi.org/10.1016/j.cell.2026.09.030

Mineral composition analysis via ICP-MS

A profile on shoot mineral contents was determined by inductively-coupled plasma mass spectrometry (ICP-MS) following the method described in Almario et al.(2017).[128] Dried shoot material ranging from 5–20 mg was digested using 500 μL of 67% (w/w) HNO_3 overnight at room temperature and subsequently placed in a 95 °C water bath for approximately 30 min until clear appearance of the solution. Samples were cooled to room temperature and then placed on ice. Subsequently, 4.5 mL deionized water was added carefully. Samples were cleared from insoluble contaminants by centrifugation at 4 °C at 2,000 x *g* for 30 min and supernatants transferred to new tubes for the following measurement. The elemental concentration was determined using Agilent 7700 ICP-MS (Agilent Technologies).

Quantification of bacterial abundance by live colony counts

Live colony counts from roots or the agar compartment were determined similarly to as previously described.[129] Briefly, roots of five-six three-week-old plants were pooled for one biological replicate, briefly washed in 10 mM $MgCl_2$, dried with sterile Whatman paper, and transferred to pre-weighed, sterilized screw-cap tubes containing metal beads. Approximately 100 mg of the agar matrix from the same square plate was harvested for the determination of live colony counts in the agar compartment. After agar and root fresh weight determination, samples were homogenized using a tissue homogenizer (Bertin Precellys; 6,200 rpm, 1 × 30 s). Subsequently, 500 μL of 10 mM $MgCl_2$ were added and the homogenization process repeated. Four serial dilutions were prepared in 96-well plates starting from a 1:10 dilution and 10 μL aliquots of each sample and each dilution were dropped onto 50% TSA plates and spread across half the plate by tilting. Plates were incubated for one-three days at 25°C until colonies were visible, and were then counted. Finally, $\log_{10}$ transformed values of determined CFUs per g sample (root or agar) per mL were displayed.

Ex planta Fe(III) reduction assay using bacterial cells

Assay medium was prepared from half-strength MS, supplemented with 400 μM ferrozine and 0.01 × artificial root exudates,[84] and buffered with 10 mM HEPES (pH 7.4) or 5 mM MES (pH 5.7). pH was adjusted with 1 M KOH, and medium was filter-sterilized (pore size <0.22 μm). Bacterial cells (IT466 or SynCom strains) were harvested by centrifugation (4,000 × g, 10 min, room temperature), washed twice with 10 mM $MgCl_2$, and resuspended in the same solution. OD_{600} was measured, and bacteria were added to the assay medium at a final OD_{600} = 0.1, containing 100 μM freshly precipitated Fe(III) (supplied as $FeCl_3$). A corresponding volume of 10 mM $MgCl_2$ served as the axenic control and IT466 cells boiled for 60 min at 99°C served as the heat-killed control to account for carry-over Fe from pre-cultivation in nutrient-rich medium.

EDTA, ascorbic acid, and coumarins used in this study were obtained from commercial sources, while sideretin was custom-synthesized by Orgentis Chemicals GmbH (Gatersleben, Germany). Compounds were prepared as 100 mM stocks: coumarins in DMSO, Na_2EDTA and ascorbic acid in sterile deionized water, and were aliquoted to avoid repeated freeze-thaw cycles. As sideretin is sensitive to air oxidation[34] and was not reduced prior to each use, it is expected to have been present as a mixture of reduced and oxidized forms; however, we termed it sideretin-hydroquinone for simplicity reasons. Sideretin-quinone was enriched by incubation of the custom-synthesized sideretin under aerobic conditions with palladium(II) as a catalyst and termed sideretin-quinone for simplicity reasons.

Compounds were added to the assay medium at 50 μM final concentration. Mock treatments consisted of a 1:1 mixture of DMSO and deionized water, and appropriate background controls (either water or DMSO) were added to each treatment to maintain equal background for each condition. Assays were incubated in a 96 well plate format at room temperature in the dark for up to 24 h. At defined time points, samples were mixed, aliquots taken and bacterial cells and insoluble Fe were removed by centrifugation (4,000 × g, 5 min, room temperature). The soluble Fe^{2+} in the remaining supernatants was quantified via the ferrozine-Fe^{2+} complex, measuring absorbance at 562 nm (Tecan Infinite 200 Pro). Absolute Fe^{2+} concentrations were determined using a freshly prepared Fe^{2+} standard curve (0–100 μM $FeSO_4$) in assay medium with 400μM ferrozine and the corresponding pH buffer. The same procedure was followed for experiments with IT466 wt and different mutants or the three different SynComs.

Ex planta Fe mobilization assay using bacterial culture supernatants

Fe-limiting cultures of IT466 to capture Fe-mobilizing compounds in the supernatants were prepared similar to as described previously.[84] IT466 wt and Δ*pvdD* were pre-cultured in ½ MS medium without Fe and supplemented with artificial root exudates and vitamins to mimic the carbon-rich but Fe-limited root environment at pH 7.4 and to induce bacterial secretion of Fe-mobilizing compounds e.g. siderophores. Supernatants of comparably grown bacterial genotypes were harvested and applied to fresh ½ MS medium containing immobile Fe(III) supplied as 100 μM $FeCl_3$, pH 7.4 with 10 mM HEPES, in the presence or absence of fraxetin, esculetin, EDTA and sideretin or scopoletin, or mock (water:DMSO, 1:1). IT466 Fe-limited culture supernatant-mediated Fe mobilization was determined from the mock condition. Different compounds were incubated in the absence of IT466 supernatants to assess compound-mediated Fe mobilization.

All compounds were added at 100 μM to the assay solution and incubated axenically, in presence of IT466 wt or Δ*pvdD* for 6 hours. At 6 hpi, insoluble Fe precipitates were removed by centrifugation (4,000 × g, 10 min, room temperature), a final concentration of 1 mM ferrozine applied and incubated for 1 hour, and the mobile fraction of Fe^{2+} quantified via the ferrozine-Fe^{2+} complex by measuring the absorbance at 562 nm using a Fe(II) standard curve as described above. Subsequently, mobile Fe^{3+} was reduced by addition of 10 mM HCl and 2.5 mM ascorbic acid. Incubation took place until saturation of the reaction for approximately 15 hours

in the dark and total mobile Fe (sum of Fe^{2+} and Fe^{3+}) determined spectrophotometrically via the ferrozine-Fe^{2+} complex. Absolute Fe^{2+} concentrations before and after Fe^{3+} reduction were determined using a freshly prepared Fe^{2+} standard curve (0–100 μM $FeSO_4$) in assay medium with 1 mM ferrozine and the corresponding pH buffer. The fraction of Fe^{3+} was calculated by subtracting the amount of mobilized Fe^{2+} from the amount of total mobile Fe. Dilution factors due to reagent addition were considered in the calculations for quantification of the different Fe species. In contrast to the previous assay with bacterial cells, ferrozine was not present during the incubation period with immobile Fe.

Ex planta PVD fluorescence measurements and siderophore activity from Fe-limited bacterial culture supernatants

Fe-limiting cultures of IT466 for PVD fluorescence and siderophore activity were prepared and analyzed as described previously, with minor modifications.[84] The OD_{600} of Fe-limited IT466 wild-type and Δ*pvdD* cultures was recorded prior to harvesting supernatants by centrifugation at 4,000 × g for 10 min. Relative PVD fluorescence units (RFU) were determined with excitation at λ_ex = 400 nm and emission at λ_em = 465 nm. RFUs were normalized to the OD_{600} of each culture for data presentation.

Siderophore activity was quantified using the chrome azurol sulfonate (CAS) assay, a colorimetric method that detects Fe(III)-chelating activity in bacterial supernatants by monitoring the decrease in absorbance at 636 nm.[130] Briefly, 20 μL of each supernatant was applied to 100 μL of CAS assay solution, and the absorbance of the blue Fe(III)-CAS-HDTMA complex at 636 nm was measured kinetically. At the time point corresponding to reaction completion for IT466 wt, Fe(III)-chelating capacity was calculated using the following formula:

$$\text{Iron} - \text{mobilizing capacity}\left(\frac{\mu\text{M Fe}}{\text{OD}_{600}}\right) = \left(\frac{\left(\frac{Abs636(Medium) - Abs636(Sample)}{Abs636(Medium)}\right) * 2}{(Volume(Supernatant) * OD600)}\right).$$

Establishment of an IT466 mini-Tn5 insertion mutant library

IT466 was conjugated with *E. coli* S17 λpir carrying pUTmTn5Km2[100] at a 1:1 ratio (final OD_{600} = 0.1 each) and co-cultivated overnight on 50% TSA (1.5% Bacto agar, BD) at 25°C. Conjugation patches were resuspended in 50% TSB and stored at -80°C in 30% glycerol. For library construction, conjugations were plated on 50% TSB containing 50 μg ml^{-1} kanamycin and 50 μg ml^{-1} nitrofurantoin and incubated at 25°C for 48 h. Individual colonies were then inoculated into 100 μl of 50% TSB with the same antibiotics in 96-well plates, incubated at 25°C with shaking at 180 rpm for 48 h, and stored at -80°C in 30% glycerol. The mutant library includes approximately 6,000 mTn5 insertion mutants of IT466. The pooled conjugation mixture was then used for the forward genetic *in vitro* screen to isolate IT466 mTn5 insertion mutants with reduced menadione-dependent Fe(III) reduction.

Forward genetic screen for IT466 mTn5 insertion mutants with diminished menadione-mediated Fe(III) reduction

The mTn5 insertion library of IT466 was screened for mutants with diminished menadione-dependent Fe(III) reduction using an agar-overlay based system adapted from Light et al. (2018).[131] In this assay, IT466 colonies are surrounded by a pink Fe- and ferrozine-dependent halo only in presence of menadione but not in presence of the solvent control DMSO (Figure S10A). Briefly, 50% TSA were prepared (1.5% Bacto Agar, Difco) and buffered with 5 mM MES to pH 5.7; supplemented with freshly precipitated Fe(III), supplied as 100 μM $FeCl_3$, and 100 μM menadione. The IT466 conjugation was streaked at a dilution to obtain approximately 100 separated single colonies per plate and 50 μg/mL kanamycin added for positive selection of IT466 strains carrying an mTn5 insertion and 50 μg/mL nitrofurantoin for negative selection of the donor *E. coli* strain carrying the mTn5 vector. Bacteria were cultivated for two days until single colonies appeared. A 10 mL overlay was applied which consisted of a ½ MS basis (without Fe) and was supplemented with 1mM ferrozine and 0.8% Difco Technical Agar, BD (minimal Fe background). A total number of approximately 4,000 colonies was phenotypically screened. Colorimetric change, visible as a pink halo around colonies, resulting from ferrozine binding to Fe^{2+} was visually tracked visually for ~6 hours. Colonies with diminished or reduced colorimetric change were isolated and the process of isolation was repeated three times to ensure contamination-free isolation of individual mTn5 insertion mutants. After three additional rounds of validations using the agar-overlay assay, the location of the mTn5 insertions in the remaining candidates was determined via TAIL-PCR (Table S2).

Identification of mini-Tn5 insertion sites

Chromosomal mTn5 integration sites were determined using two consecutive PCRs (TAIL-PCR) as described previously.[100,132] For the first PCR, 10 ng of genomic DNA was amplified with primers MM003/MM004 using Super-Taq DNA polymerase (Bioron) under the following conditions: 94 °C for 2 min; 6 cycles of 94 °C for 30 s, 30 °C for 30 s, and 72 °C for 1 min; followed by 30 cycles of 94 °C for 30 s, 45 °C for 30 s, and 72 °C for 1 min; and a final extension at 72 °C for 10 min. For the second PCR, a 1:10 dilution of the first PCR product was amplified with primers MM001/MM002 under the following conditions: 94 °C for 2 min; 30 cycles of 94 °C for 30 s, 57 °C for 30 s, and 72 °C for 1 min; and a final extension at 72 °C for 10 min. PCR products were separated by agarose gel electrophoresis, and a dominant band of Sanger-sequencing-compatible size was excised and sequenced using primer MM001 (Eurofins Genomics). Sequencing results were analyzed with CLC Main Workbench (QIAGEN).

Please cite this article in press as: Malisic et al., *Arabidopsis* uses distinct coumarins and bacterial pathways for pH-adaptive iron acquisition, Cell (2026), https://doi.org/10.1016/j.cell.2026.09.030

Targeted mutagenesis in IT466

Marker-free deletion mutants in IT466 were generated as described previously.[84] Target genes included *pvdD* (IT466_gene_2009), *roxR* (IT466_gene_3943), *roxS* (IT466_gene_3942), the *roxSR* operon (IT466_gene_3942-3943), *anr* (IT466_gene_3657), the petCBA (IT466_gene_4378-4380) and *ccoNOQP-1* and *ccoNOQP-2* operons (IT466_gene_3640-3647). Upstream and downstream flanking regions (~750 bp) of each target gene were amplified and assembled into the linearized pK18mobsacB suicide vector[117] (GenBank: FJ437239.1) using HiFi assembly. Plasmids were first transformed into *E. coli* BW29427 (DAP auxotroph), and correct insertion of the target flanking regions was verified by colony PCR. Plasmids were subsequently conjugated into the recipient strain IT466 using E. coli BW29427 as the donor in the presence of 50 μg ml^{-1} DAP. Transformants were selected with 50 μg ml^{-1} kanamycin (plasmid marker) and 50 μg ml^{-1} nitrofurantoin (IT466-specific resistance), while counter-selecting the donor by omitting DAP. Chromosomal integration of the plasmid was confirmed by colony PCR using primers spanning the plasmid and chromosomal flanking regions. Deletion mutants were generated via sucrose counter-selection (10% w/v), triggering a second homologous recombination event. Clean deletions were verified by colony PCR of the 5′ and 3′ flanking regions, using primers binding ~100 bp outside the previously amplified regions, followed by Sanger sequencing.

In vitro bacterial growth kinetics

IT466 wt and *roxSR*-related mutants were pre-cultured for 48 hours in 50% TSB at 25°C under agitation (180 rpm). Cultures were then diluted to an initial OD_{600} of 0.05 in fresh 50% TSB. Growth was monitored by measuring the absorbance at 600 nm every hour for 48 hours using a microplate reader (Tecan Infinite 200 Pro).

Bacterial growth at different oxygen concentrations

IT466 wt, the *roxR*::mTn5 transposon mutant, and the chromosomal deletion mutants Δ*anr*, Δ*roxR*, Δ*roxS*, Δ*roxSR*, Δ*petCBA*, Δ*ccoNOQP-1* Δ*ccoNOQP-2* (Δ*cco-1* Δ*cco-2*) were pre-cultivated in 50% TSB for 2 days at 25°C and 180 rpm agitation speed. Cells were harvested by centrifugation at 4,000 x *g* for 10 minutes, washed with 10 mM $MgCl_2$ and resuspended in the same solution. OD_{600} was assessed and bacterial genotypes diluted to an OD_{600} = 1 in 10 mM $MgCl_2$. Bacteria or a 10 mM $MgCl_2$ control inoculated into fresh 50% TSB medium at a final OD_{600} of 0.05 and incubated for 96 hours in air tight chambers at three different oxygen concentrations (oxic: 20.9% O_2; microoxic: 8%–9% O_2; near anoxic: < 0.04% O_2) within airtight chambers for 96 hours. Oxygen was depleted using a crystalline silica-based carrier material according to the manufacturer's instructions (Anaerocult® A, Merck). O_2 concentration was measured by a digital O_2 sensor within each chamber. At 96 hpi, OD_{600} was assessed.

RNA sequencing for bacterial transcriptomics

The experiment was performed as described in the *ex planta* Fe(III) reduction assay using bacterial cells section. Each IT466 genotype was treated with sideretin or DMSO as mock and IT466 wild type was additionally treated with fraxetin (Table S3). Cells from IT466 wild type, *roxR*::mTn5 and Δ*roxR* were harvested by centrifugation (4,000 x g, 10′, 4°C) and frozen in liquid nitrogen at 3 hpi, where differential responses in Fe(III) reduction between mutants and IT466 wild type begin to appear. Bacterial cells were lysed, and RNA was extracted with Trizol® Reagent (Ambion, Life Technologies) followed by purification using the ReliaPrep™ RNA MiniPrep Systems kit (Promega) according to the manufacturers' instructions. RNA was subjected to the Novogene Illumina sequencing pipeline including mRNA library preparation and rRNA depletion (NovaSeq X Plus Series (PE150)).

Acquired reads were trimmed with fastp (v 0.23.4),[110] using a quality threshold of 25 and a window length of 5. For differential transcript analysis, reads were then aligned to the IT466 genome with the HISAT2 (v 2.1.0),[111] using default settings except for the "–no-spliced-alignment" option. To examine the potential effect of the *roxR*::mTn5 insertion on the *roxR* protein product, we also aligned reads against the *roxR*::mTn5 genome using HISAT2 and deduced the amino acid sequence based on *in silico* translation of the mapped reads.

featureCounts (v2.0.2)[112] was used to assign reads to genes (Table S5). DESeq2[113] was used to identify differentially expressed genes, using a cutoff threshold of |log2 fold change| > 1 and adjusted $p < 0.05$ (Tables S7–S9).

To identify genes showing transcriptional interactions between coumarins and *roxR*, we used two approaches. First, an interaction analysis using a design formula of ~ genotype*treatment was used, and contrasts were set up such that a positive log_2 fold change indicates that sideretin treatment leads to a relatively increased expression of the gene in IT466 wt compared to the given mutant (Table S10). As a second approach, we identified DEGs that significantly respond to sideretin in IT466 wt but not the *roxR* mutants, and do not show significant expression differences between IT466 wt and the mutants in the absence of sideretin.

For hierarchical clustering analysis, read counts were normalized with DESeq2 based on the estimateSizeFactors function, log_2 transformed, and z-scaled, before hierarchical clustering with SciPy[114] (Table S11).

For GO term enrichment, GO annotations were mapped to the IT466 genes using two methods. Firstly, IT466 loci were mapped to *Pseudomonas aeruginosa* PAO1 genes using KO terms from the KEGG website, and the corresponding GO terms from the Gene Ontology Consortium (2026-01-23 release)[133] were assigned to the IT466 genes (Table S12). In case of ambiguity, only GO terms assigned to all PAO1 genes from a particular KO term were used. Secondly, deduced amino acid sequences for IT466 loci were analyzed with InterProScan (v5.76-107.0).[115] The union of GO terms from each method was used for GO enrichment analysis using TopGO.[116]

Please cite this article in press as: Malisic et al., *Arabidopsis* uses distinct coumarins and bacterial pathways for pH-adaptive iron acquisition, Cell (2026), https://doi.org/10.1016/j.cell.2026.09.030

Root exudate collection

Root exudates were collected from plants pre-grown axenically for 9 days on half-strength MS medium containing vitamins and sucrose. Plants were then transferred to plates with contrasting Fe conditions (100 μM $FeCl_3$ or Fe-EDTA), buffered with 5 mM MES (pH 5.7) or 10 mM HEPES (pH 7.4), and cultivated for 5 additional days under germ-free (axenic or heat-killed), or live bacterial conditions (initial OD_{600} = 0.0001). Roots from three to six intact seedlings were briefly washed with sterile deionized water, and seedlings were placed in non-transparent 96-well plates containing 0.1 mM $CaCl_2$ solution buffered to pH 5.7 (5 mM MES) or pH 7.4 (10 mM HEPES). Plates were incubated in a light chamber for 6 h to allow accumulation of root exudates. Exudates were transferred to fresh tubes, and insoluble material was removed by centrifugation for 5 min at 4,000 × g and 4°C. Samples were frozen in liquid nitrogen and stored at −80°C until analysis by ultra-performance liquid chromatography high-resolution mass spectrometry (UPLC-HRMS).

Mass spectrometry measurements for coumarin quantification

Root exudate samples were subjected to UPLC-HRMS analysis using a Vanquish™ UHPLC system coupled to a Q Exactive Plus Mass Spectrometer (Thermo Fisher Scientific). A reversed phase Acquity UPLC® HSS T3 Column (100 Å, 2.1 mm x 150 mm, 1.8 μm, Waters) and an Acquity UPLC® HSS T3 VanGuard Pre-column (100 Å, 2.1 mm x 5 mm, 1.8 μm, Waters) were used for coumarins baseline resolution. A mobile phase (A: Water + 0.1 % formic acid; B: Acetonitrile + 0.1 % formic acid) gradient was applied as follows: 0 min to 0.5 min 10% solvent B; linear increase of solvent B to 80% from 0.5 to 8 min. All coumarins were eluted within five min. Additional steps were included to guarantee both column wash and equilibration. The column temperature was set to 30 °C and the flow rate to 0.4 mL min^{-1}. The injection volume was 5 μL. The MS system was equipped with a HESI source operating in both positive and negative ion mode. The source values were set in positive mode as follows: spray voltage 3.5 kV; capillary temperature 255°C; S-lens RF level 40; aux gas heater temperature 400°C; sheath gas flow rate 40; aux gas flow rate 10. In negative mode, the spray voltage was set to 2.5 kV, the sheath gas flow rate to 47 and the aux gas flow rate to 11. A full MS ddMS2 experiment was performed for spectra acquisition. The resolution in the full scan was set to 70,000. For MS/MS experiments a resolution of 17,500 and an NCE of 30 V was used. MS data were acquired and processed by the Trace Finder Software (v. 4.1, Thermo Fisher Scientific, Germany). Compound quantification was performed based on an external calibration curve. A stock solution with a final concentration of 0.8 μg/mL of all coumarins analyzed in this study was prepared. The calibration standards were prepared by serial dilution of this stock solution (μg mL^{-1}, 0.8, 0.7, 0.6, 0.5, 0.4, 0.3, 0.2, 0.1, 0.05, and 0.025). To generate the calibration curve, the peak area on the extracted ion chromatogram (XIC) of the deprotonated or protonated molecule ion was measured. A least-square linear regression was used to best fit the linearity curve. A summary of retention times and multiple reaction monitoring (MRM) transitions for the analyzed coumarins is provided in Table S13.

QUANTIFICATION AND STATISTICAL ANALYSIS

Data were analysed in the RStudio environment of R programming language and with python. Each dataset was first tested for normality using the Shapiro-Wilk test. Because all datasets either showed non-parametric distributions or had sample sizes smaller than 30, preventing confident assessment of normality, non-parametric tests were applied. For comparisons involving more than two groups, either a Kruskal-Wallis test followed by Dunn's post hoc test for pairwise comparisons, or a Kruskal-Wallis test followed by pairwise Wilcoxon rank-sum tests with Benjamini-Hochberg correction for multiple comparisons, was used. For comparisons between two groups, a Wilcoxon rank-sum or Welch's test was applied, with Benjamini-Hochberg correction when multiple pairwise tests were performed. The specific statistical tests used for each dataset are indicated in the corresponding figure legends.